INSTITUTO SUPERIOR DE ENGENHARIA DE LISBOA
Área Departamental de Engenharia Mecânica
ISEL

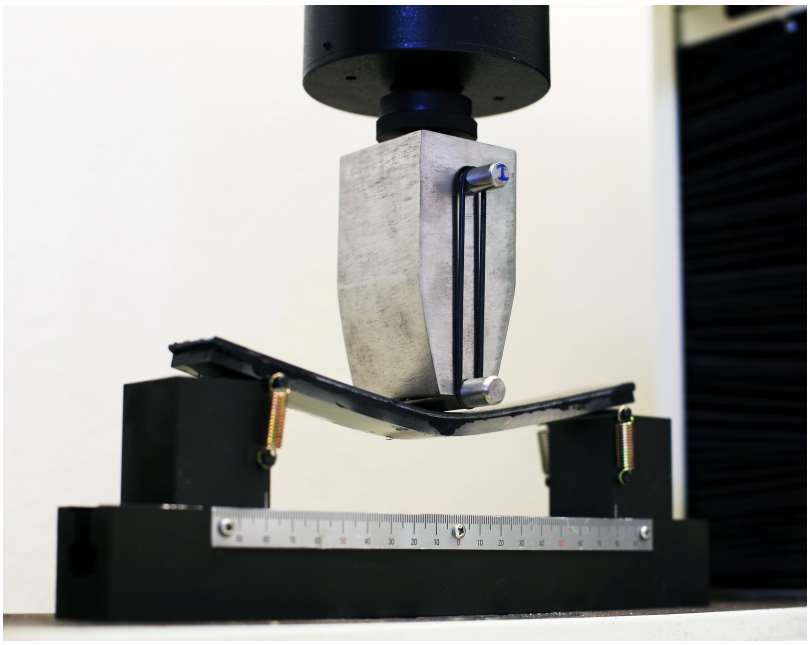

Experimental and Numerical Analysis of Two-Layer Composite Beams

TIAGO JORGE PINTO ARAÚJO
Licenciado em Engenharia Mecânica

Trabalho Final de Mestrado para obtenção do grau de Mestre
em Engenharia Mecânica: Manutenção e Produção

Orientadores:
Doutor Hugo Alexandre Freixial Argente dos Santos, ISEL
Mestre Afonso Manuel da Costa de Sousa Leite, ISEL

Júri:
Presidente: Doutora Maria Teresa Moura e Silva, ISEL
Vogais: Doutora Rosa Marat-Mendes, ENIDH (Arguente)
Doutor Hugo Alexandre Freixial Argente dos Santos, ISEL (Orientador)

Dezembro de 2019

PÁGINA INTENCIONALMENTE DEIXADA EM BRANCO

INSTITUTO SUPERIOR DE ENGENHARIA DE LISBOA
Área Departamental de Engenharia Mecânica
ISEL

Experimental and Numerical Analysis of Two-Layer Composite Beams

TIAGO JORGE PINTO ARAÚJO
Licenciado em Engenharia Mecânica

Trabalho Final de Mestrado para obtenção do grau de Mestre
em Engenharia Mecânica: Manutenção e Produção

Orientadores:
Doutor Hugo Alexandre Freixial Argente dos Santos, ISEL
Mestre Afonso Manuel da Costa de Sousa Leite, ISEL

Júri:
Presidente: Doutora Maria Teresa Moura e Silva, ISEL
Vogais: Doutora Rosa Marat-Mendes, ENIDH (Arguente)
Doutor Hugo Alexandre Freixial Argente dos Santos, ISEL (Orientador)

Dezembro de 2019

PÁGINA INTENCIONALMENTE DEIXADA EM BRANCO

Agradecimentos

Como autor do presente texto pretendo expressar os meus agradecimentos a todas as pessoas que ajudaram à sua elaboração, seja esse apoio de carácter académico ou pessoal.

Agradeço ao meu orientador, Professor Hugo Santos, pela oportunidade do tema proporcionado, pelo apoio e paciência prestadas à estrutura do trabalho e pelas reuniões muito úteis e esclarecedoras, fundamentais para a realização desta dissertação.

Agradeço ao meu co-orientador, Professor Afonso Leite, por todo o apoio e motivação prestados, pela constante disponibilidade em responder às variadas dúvidas, pela informação a nível de software utilizado, preparação de amostras a ensaiar e respetiva análise de resultados.

Agradeço à empresa Steel Cash, Lda (Leiria), por ter apresentado disponibilidade rápida no fornecimento do aço para produção da peça do dispositivo de flexão essencial à realização da prática experimental.

Ao grupo Sofrapa, nomeadamente à retificadora Auto Costa (Viseu), por ter colaborado com a maquinação da peça do dispositivo de flexão e do varão de aço inox que completa o mesmo.

Um grande obrigado à empresa Dustrinox, Lda (Alverca), por ter fornecido parte do material a ensaiar, nomeadamente as amostras de aço e alumínio.

Agradeço à Gilda Maria, que disponibilizou parte do seu tempo para ajudar com as fotos obtidas no ensaio experimental, essenciais para obter os ângulos de rotação das vigas.

Agradeço à Sandra de Freitas, pelas dicas e opiniões dadas, pela motivação e carinho prestado.

Agradeço aos meus pais, Olga Pinto e Jorge Araújo pela confiança e esperança que sempre me depositaram e sobretudo pela educação que me incutiram, sem a qual não estaria onde estou hoje.

Agradeço à minha família por todo o apoio e incentivo, aos amigos chegados, pela amizade e ajuda mútua nos períodos mais críticos e a todos aqueles que de forma direta ou indireta influenciaram nas minhas escolhas e caminhos a seguir, um enorme obrigado.

Resumo

Os materiais compósitos têm desempenhado um papel importante em muitas aplicações de diferentes áreas na prática de engenharia. Devido às suas propriedades mecânicas e à possibilidade de serem projetadas para uma finalidade específica, as vigas laminadas em particular são de enorme interesse há várias décadas. O uso deste tipo de materiais é cada vez mais frequente. O facto de apresentarem propriedades mecânicas optimizadas provenientes da combinação de diferentes materiais é o factor-chave que justifica a procura existente pelas mais variadas indústrias. Devido a esta procura é conveniente que na fase de projeto sejam avaliados parâmetros mecânicos, de maneira a obter estruturas capazes consoante a sua finalidade. Desta forma, torna-se útil a investigação tanto experimental como numérica do comportamento mecânico do conjunto de camadas, tendo em consideração a interação das camadas, a sua geometria e as suas propriedades mecânicas. De entre os vários processos para efetuar a análise experimental, o ensaio de flexão é amplamente utilizado na maioria dos casos.

O objetivo deste trabalho é estudar experimentalmente e numericamente o comportamento mecânico de vigas laminadas compósitas ligadas por um adesivo. Três configurações distintas de materiais (aço-alumínio, aço-polímero e alumínio-polímero) e dois adesivos de natureza diferente foram considerados para avaliação. Diferentes espessuras de camadas foram apresentadas de acordo com o material considerado. Os resultados foram gerados a partir de dois métodos de análise diferentes. Em primeiro lugar por uma abordagem numérica, nomeadamente por um modelo de equilíbrio FEM disponível. Em segundo lugar, realizou-se um ensaio de flexão de três pontos para a obtenção dos resultados experimentais.

O modelo numérico de equilíbrio FEM em questão é baseado nas consideraçõs de Timoshenko ou Teoria da Deformação de Corte de Primeira-ordem (FSDT), de maneira que o efeito de corte entre camadas seja levado em consideração. Toda a manipulação e análise feitas nas vigas laminadas compósitas serão consideradas dentro do regime linear elástico. Os resultados mostram, por um lado, a capacidade do modelo numérico conseguir prever, com algum rigor, o comportamento mecânico das vigas laminadas compósitas. Por outro lado, a origem de erros mais relevantes no caso das vigas ligadas com resina epoxy, devido à impossibilidade de avaliar os parâmetros mecânicos do adesivo assumidos pelo modelo.

Palavras-chave

Vigas de duas camadas
Teoria de Timoshenko
Análise experimental
Deslizamento entre camadas
Ensaio flexão de três pontos
Modelação numérica via FEM

Abstract

Composite materials have played an important role in many applications from different fields in engineering practice. Due to their mechanical properties and the possibility of being designed for a specific purpose, layered beams, in particular, have been of enormous interest for several decades. The use of this type of materials is becoming more frequent. The fact that they present optimized mechanical properties from the combination of different materials is the key factor that justifies the demand for the most varied industries. Due to this demand, it is convenient that in the design process, the parameters are evaluated to obtain capable structures according to their purpose. Thus, it is useful to investigate both experimental and numerical mechanical behaviour of the layer set, considering the layers interaction, their geometry and their mechanical properties. Among the several methods to perform this type of evaluation, the bending test is widely used in most cases.

The aim of this work is to study experimentally and numerically the mechanical behaviour of laminated beams composed by two-layers connected by an adhesive. Three different material configurations (steel-aluminium, steel-polymer and aluminium-polymer) and two adhesives of different nature were considered for evaluation. Different layer thicknesses were presented according to the considered material. Results were generated from two different analysis methods. Firstly by a numerical approach, namely by an available equilibrium FEM model. Secondly, a three-point bending test was performed to obtain the experimental results.

The concerned equilibrium FEM numerical model is based on Timoshenko's assumptions or First-order Shear Deformation Theory (FSDT), so the shear effect in the interlayer slip is taken into account. All the manipulation and analysis made to laminated composite beams will be considered within the linear elastic regime. The results show, on the one hand, the ability of the numerical model predict with some accuracy the mechanical behaviour of laminated composite beams. On the other hand, the origin of more relevant errors in the case of epoxy bonded beams, due to the impossibility to evaluate the mechanical parameters of the adhesive assumed by the model.

Keywords

Two-layer beams
Timoshenko theory
Experimental analysis
Interlayer slip
Three-point bending test
Numerical modeling via FEM

Contents

List of Figures

List of Tables

Abbreviations

3PB	*Three-Point Bending*
ASTM	*American Society for Testing and Materials*
FEM	*Finite Element Method*
FSDT	*First-order Shear Deformation Theory*
ISO	*International Organization for Standardization*
PMMA	*Polymethylmethacrylate*

Nomenclature

δ	Displacements of the mid-span	[mm]
θ	Rotation angle	[º]
ν	Poisson's coefficient	[-]
ν_a	Poisson's coefficient of layer a	[-]
ν_b	Poisson's coefficient of layer b	[-]
ρ	Mass density	$[kg/m^3]$
σ_u	Ultimate tensile strength	[Pa]
σ_y	Yield strength	[Pa]
b	Width of beam	[mm]
$Config.$	Material configuration	[-]
E	Young's modulus	[Pa]
E_a	Young's modulus of layer a	[Pa]
E_b	Young's modulus of layer b	[Pa]
F	Applied force in the mid-span	[N]
F_{nom}	Nominal applied force	[N]
G	Shear modulus	[Pa]
G_a	Shear modulus of layer a	[Pa]
G_b	Shear modulus of layer b	[Pa]
H_a	Thickness of layer a	[mm]
H_b	Thickness of layer b	[mm]
H_t	Total thickness of the beam	[mm]
H_{tepoxy}	Total thickness of the beam with epoxy resin	[mm]
H_{tpecol}	Total thickness of the beam with Pecol MSP 50	[mm]
L	Distance between the supports	[mm]
L_t	Total length of beam	[mm]
$L/2$	Distance between the support and the mid-span	[mm]
ks	Interlayer slip modulus	[Pa]
SD_δ	Standard deviation of displacement	[mm]
SD_θ	Standard deviation of rotation angle	[º]

Chapter 1

Introduction

1.1 Motivation and Goal

The combination of different materials has a key role in various industries such as mechanical, civil, automotive, aerospace, naval, biomedical, and other engineering areas. There is an increasing demand for new, intelligent and multifunctional materials and composite structures are a welcoming solution for this type of requirement. Composite materials consist of building up a single unit by using subelements of different materials that are connected through shear connectors or adhesives. Several reasons justify the use of these materials, namely, the possibility of weight reduction, the need for higher stiffness and strength of the structure, enhanced fracture, fatigue and corrosion properties, and, last but not least, the cost reduction.

Nowadays, some current examples of these material combinations can be found in several industries. In particular, the sandwich-beams, which are often used in vehicle and airplane construction, refrigeration and building engineering. The timber-concrete beams are a widely used solution in civil construction as well. The increasing use of glass and carbon fiber reinforced polymers in cars, boats and airplanes design is proof that composite materials are gaining its space in engineering applications [1].

Hereupon, it is noticeable that in certain applications the product design requires systems that are made of more than one material. It is on these systems that this study will focus, more specifically on laminated composite beams.

Through this kind of research work, it is possible to extrapolate the behaviour of a set of materials on a smaller scale to higher scales and varied applications. Having said that, it is noticeable a significant evolution in all industries due to the appearance of new material combinations with increasingly attractive mechanical properties.

1.2 Problem Description

With the goal of studying the mechanical behaviour of laminated beams, sets of two-layers connected by an adhesive will be considered, and different material configurations will be tested. On one hand, the numerical results will be obtained from the equilibrium finite element model proposed in [2], which is based on Timoshenko's assumptions. On the other, the experimental results will be obtained by performing a three-point bending test (3PB). Similarly to the numerical model, the equivalent laminated beam set will be subjected to a concentrated force with variable intensity, applied in the mid-span of the beam, under quasi-static conditions, to obtain the corresponding displacements. The beam model adopted in this work was designed by using ANSYS software.

Three different material configurations will be analyzed, namely Steel S235JR/Alloy 5754; Steel S235JR/Polymethylmethacrylate (PMMA) and Alloy 5754/Polymethylmethacrylate (PMMA). The PMMA under consideration is based on a standard setacryl and polarlite sheets, produced by [3]. Additionally, two adhesives of different nature will be tested, epoxy resin and an insulating glue, specifically. These materials were chosen because they present a different Young modulus between each other, the same thought was given with the choice of adhesives. Considering the analysis in the linear elastic regime, some conclusions will be drawn through the comparison of both, numerical and experimental results.

1.3 Thesis Structure

The present thesis is divided into six chapters, including the Introduction.

Chapter II contains the State-of-the-Art, which begins by describing two existing beam theories, namely the Euler-Bernoulli and Timoshenko beam theories. Moreover, it establishes a retrospective view of composite beams, supported by its historical and relevant studies presented in the literature, whether in a numerical or experimental context.

In chapter III, the Experimental Procedure is presented, detailing how the laminated beam model was designed, as well as its fabrication and equipment involved in the experimental tests.

In chapter IV, the results from the numerical model and the 3PB tests are presented and consequently compared.

In chapter V, the conclusions that have been drawn through the analysis of the results of each applied method are described.

Finally, in chapter VI, some suggestions are presented for future developments related to the topic.

Chapter 2

State-of-the-Art

2.1 Composite Beams

Composite beams are widely used in many industrial applications, due to the combination of mechanical, thermal insulation, corrosion resistance, and other attractive properties. Such structures can be improved for a specific purpose and, additionally, their mechanical behaviour is much better when compared to single-layer beams. Laminated beams are a combination of two or more layers composed of different materials connected through strong adhesives or other types of shear connectors such as shear studs, nails, etc, thus forming a single unit.

The industry has been increasingly determined to replace mechanical assemblies with adhesive-bonded ones to lighten the structures and in some cases mixed assemblies (screwed/adhesive-bonded). The mechanical behaviour of composite beams is strongly affected by the interlayer slip, as so, it must be considered for a proper analysis, in order to get reliable results.

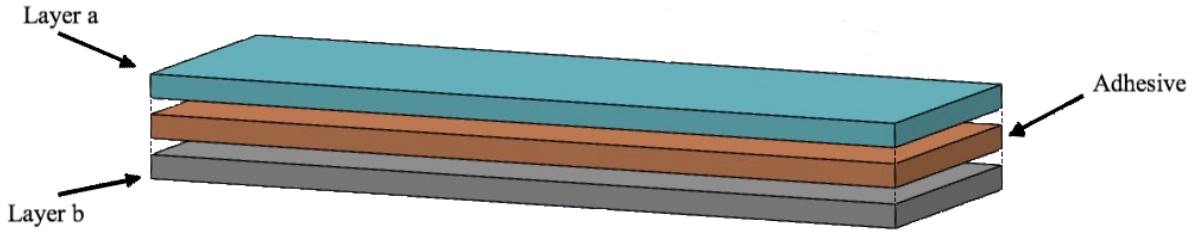

Figure 2.1: Example of a laminated beam structure.

2.2 Euler-Bernoulli Vs Timoshenko Beam Theories

For a better understanding of this work, it is convenient to know in which theory of beams this work is based on, in specific the Timoshenko beam theory. To do so, its main advantages and the comparison with the classical beam theory are discussed below.

The Euler-Bernoulli hypothesis considers that planes that are normal to the beam axis before bending remain plane and perpendicular to it after deformation. This means the Euler-Bernoulli beam theory does not consider any effect of the transverse shear deformation. Hence, the application of this beam theory to the analysis of composite beams with interlayer slip can be questioned, in particular for thick and short beams [4].

A beam theory that can handle thick beams is the so-called Timoshenko's beam theory, which assumes the effects of both, rotary inertia and shear deformation. Timoshenko's theory or First-order Shear Deformation Theory (FSDT) is still one of the most adopted beam theories that have appeared in the literature. Although Timoshenko's theory can be used to model the vibration of layered beams, this work will not take into account the rotary effect.

To illustrate both situations, see Figure 2.2, where the red-dotted and blue continuous represent the deformed configurations of a beam modelled using the Euler-Bernoulli and Timoshenko beam theory, respectively.

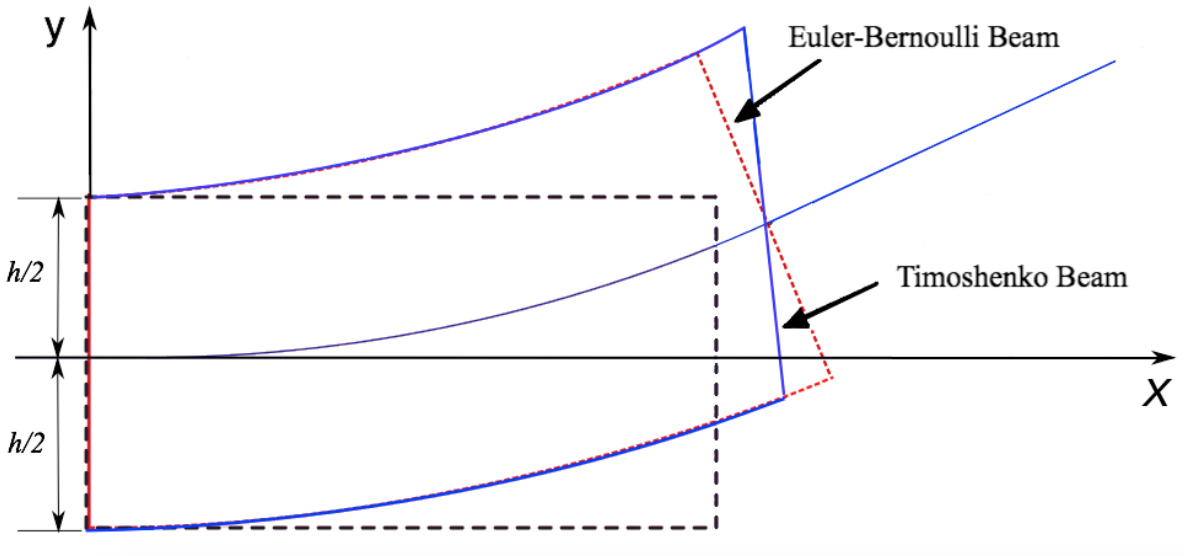

Figure 2.2: Deformed beam configurations for each beam theory.

2.3 Historical Background on the Analysis of Composite Beams

2.3.1 Numerical Models

Many efforts and a significant number of research works have been presented in the literature in the last 70 years, dedicated to this subject of numerical models of Composite Beams. The first studies were based on the assumptions of linear elastic material models and the Euler-Bernoulli hypothesis, with interlayer slip and had the purpose to investigate the mechanical behaviour of partial interaction composite beams [5, 6, 7, 8, 9].

According to many authors, Newmark [5] was the pioneer in this specific problem, developing the first mechanical model including partial interaction for beams. Newmark's work was based on a linear relationship between the slip and interlayer shear force and derived the governing equations of partial-interaction composite beams based on the Euler-Bernoulli beam theory.

Following Newmark's work, many other authors have extended this model to other problems such as beams with two or more layers [10, 11], non-linear range [6, 12, 13, 14, 15], Timoshenko two-layer beam [2, 16, 17, 18], high order theories [19, 20], etc.

However, when beams with a small span-to-depth and low shear rigidity, or continuous spans are considered, the effect of transverse shear deformation is not small, and therefore, cannot be disregarded. Significant advances in the theory of two-layer beams with partial interaction were made through the introduction of shear flexibility of both layers according to the well-know Timoshenko theory.

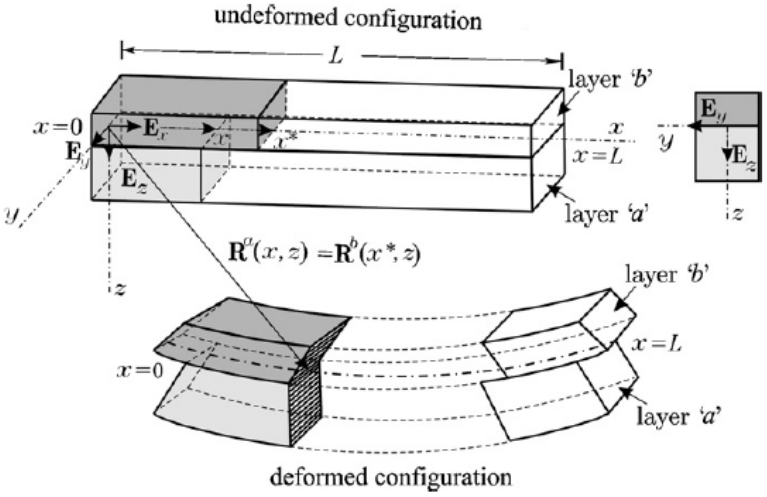

Figure 2.3: Undeformed and deformed configuration of a two-layer beam [16].

The shear deformation effect was incorporated in the analysis of composite beams for the first time by Murakami [21]. Murakami adopted Timoshenko's beam theory to analyze the effect of interlayer slip on the behaviour of laminated beams using the FEM. Recently in the literature, many authors appeared trying to develop furthermore about this problem, some of the most relevant studies are mentioned below.

In particular, Martinelli [22], proposed an analytical solution for two-layer composite beams in partial shear interaction, and also presented some expressions of stiffness matrix and equivalent nodal forces.

Schnabl [16] developed an analytical model for linear elastic behaviour of layered beams, which is based on Timoshenko's beam theory, therefore the cross-section rotations of the layers are generally different from each other.

Based on Schnabl's assumptions, Nguyen [17] proposed a new formulation based on the exact stiffness matrix for a two-layer Timoshenko composite beam with interlayer slip. The latter formulation can be used in a displacement-based procedure for the analysis of shear deformable beam with interlayer slip.

In a paper by Xu and Wu [18], the transverse shear effect was taken into account considering Timoshenko's kinematic assumptions for each layer. In order to provide a closed-form solution for static, dynamic and buckling, the authors simplified the problem by introducing a kinematic constraint where both layers are assumed to have the same transverse shear strain.

Lastly, Le Grongnec [23] presents an original closed-form expression of the elastic buckling loads of a two-layer shear-deformable beam with interlayer slip, where Timoshenko kinematic hypotheses are considered for both layers and the shear connection (no uplift is permitted).

It is remarkable how the availability of powerful computers and technology itself brought improvements in terms of research works. Thanks to this innovation, numerical methods, such as the FEM, allowed engineers to simulate and predict the behaviour of complex structural problems, such as layered structures. A large number of research works has been published, which makes numerical modelling one of the most used tools concerning mechanical behaviour analysis.

2.3.2 Experimental Procedures

Several works have been published in the literature addressing the numerical analysis of composite beams, as presented in the previous section. However, when it comes to adhesively bond dissimilar materials and understanding how they behave in practice, a short amount of works appear in the literature. Since the present work focuses on the linear elastic regime of laminated composite beams, some references of experimental nature will be presented. However, the following works meet a different range of analysis and other types of composite beams as well. Despite that, there is a commitment to investigate the behaviour of these structures, both numerically and experimentally.

The automotive industry has been showing an increasing interest in composite materials, with several published works in the literature dealing with this topic. As an example, in [24], the authors present a study where they emphasize how car body design is important in the vehicle structure, in terms of reproducing an efficient behaviour during a collision situation. Although it is a study focused on the impact resistance, layered materials play a central role. In that work, there is a commitment to present a better knowledge in joining dissimilar materials and corresponding crash behaviour. Combinations of aluminium and steel materials were considered with epoxy resin adhesives. The results between numerical simulations and experimental practices were accomplished showing a good correlation.

A similar study was also presented in [25], in which several bi-material configurations were tested. The authors support the use of adhesive bonded materials, taking into account the reduction of assembling time and number of fasteners, as well as the design of a more resistant structure. Once more, with the aid of FEM simulations and experimental tests, as represented in Figure 2.4, results were obtained and discussed.

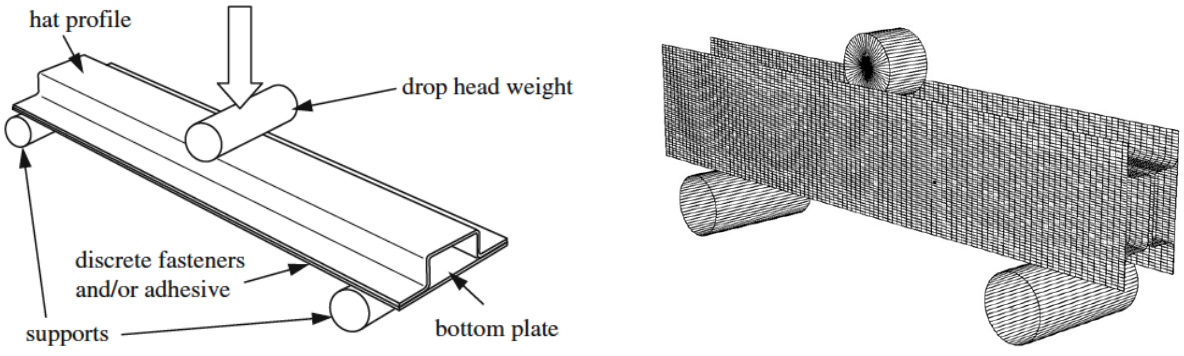

(a) 3PB test sketch.

(b) FE model.

Figure 2.4: Simulations of bi-material structures presented in [25].

Another experimental work was presented in [26], where the focus goes into the bending deformation process of two different types of metal. A composite beam was formed by two layers, one of duplex stainless steel and another of low carbon steel, with thicknesses of 3 mm and 8 mm, respectively. The obtained results from a FEM model were then compared with results from a 3PB test, to provide a reference for further forming fabrication of a bimetal composite.

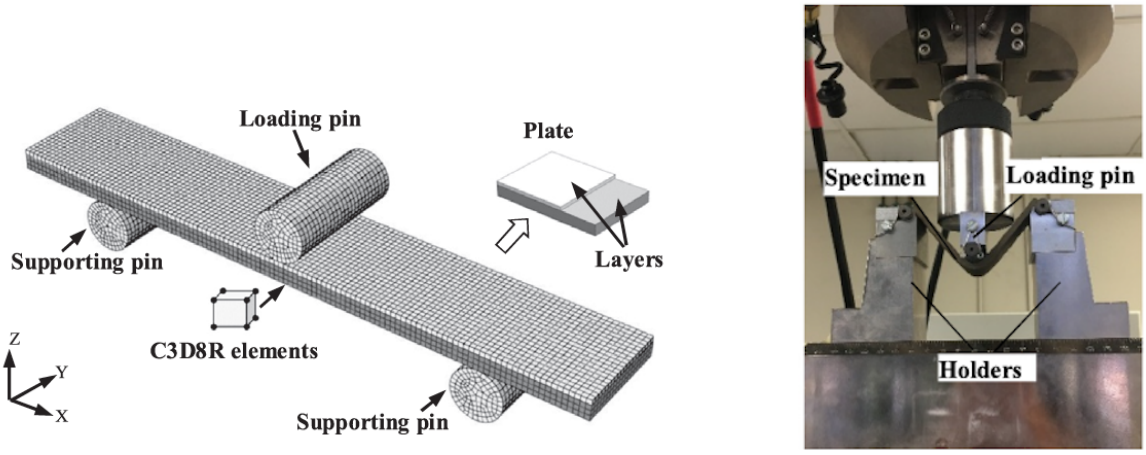

(a) FEM model analysis. (b) 3PB test.

Figure 2.5: Analysis procedures presented in [26].

The concept of the sandwich beam has become quite frequent during the last years and is often a welcome solution which follows the same pattern of experimental and analytic evaluations.

In the literature, several works can be found dealing with this specific type of composite beam. In those studies, each author has a distinct focus, for instance, in [27] the authors focus on ”honeycomb” beams through analytical and experimental analysis up to the plastic regime.

In a different approach, the study presented in [19] shows an analysis of sandwich beams taking into account higher-order theories, namely third order. In [12] the authors developed a numerical model to translate the mechanical behaviour of a five-layer beam.

These works are usually evaluated analytically, numerically and/or experimentally. In Figure 2.6 are presented the experimental practices, namely the 3PB tests performed in some of such works.

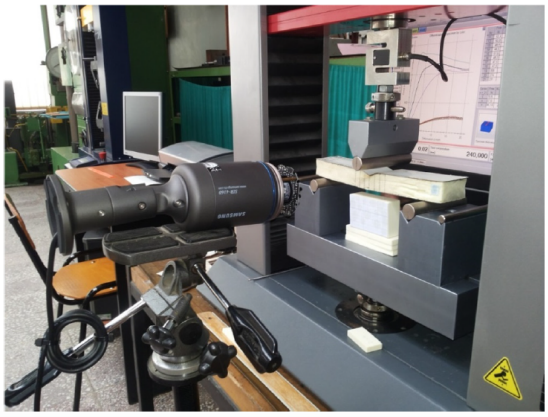

(a) Experimental practise at [19].

(b) Experimental practise at [12].

Figure 2.6: Examples of composite beams subject to the 3BP test.

When the main focus goes to the composite beam behaviour, it is crucial to consider the bonding method used to join the layers. To do so, it is important that when these layers are bonded, certain procedures are followed to prevent the assembly collapse and to understand how the interaction between layers affects the structure behaviour.

Although the present work will not focus on the fracture area in specific, some studies can be found in the literature. For instance, in [28] the authors aim to study the initiation of adhesive failure, where different surface treatments of the adhesive are considered to detect which produces best results. For this, and once again, the 3PB test was chosen as an analysis tool. Moreover, the authors explain that the substrate choice should be correctly chosen since a thick substrate increases the dispersion and a thin substrate may induce local unwelcome plastic strain.

The next chapter will expose the Experimental Procedure adopted in this work. The instrumentation and materials involved will be detailed, as well as the analysis made to the laminated composite beams, both numerical and experimental.

Chapter 3

Experimental Procedure

3.1 Test set-up and Instrumentation

Since the three-point bending (3PB) device was not complete in the facilities of the Mechanical testing laboratory of the Mechanical Engineering Department of ISEL (only its lower testing apparatus was available), it was necessary to carry out the design and construction of its upper part, so that the experimental work would be possible. To achieve that, a block of steel was purchased to complement the system, being its material composition and technical drawing presented in Appendices A.1 and A.2. Figure 3.1 shows the 3D model designed using SOLIDWORKS[1] software.

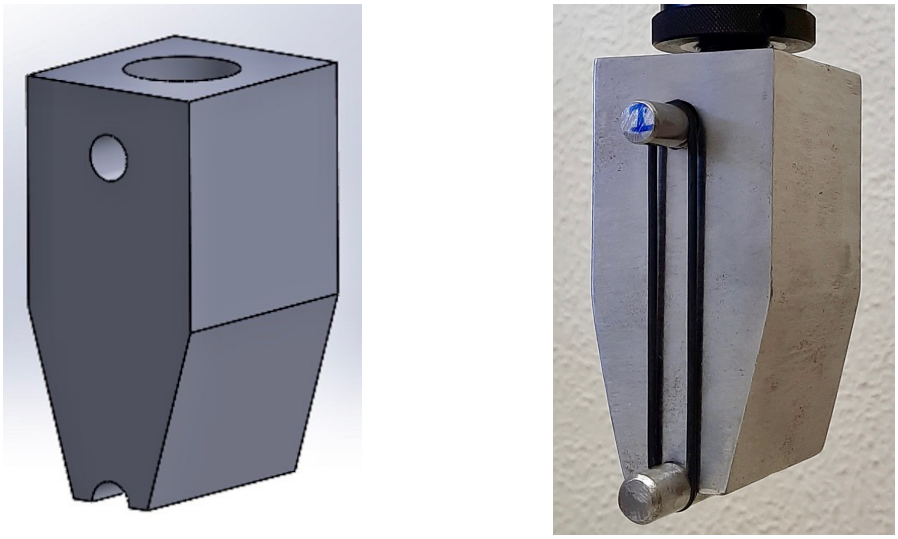

(a) 3D model. (b) Final look of the device.

Figure 3.1: Upper part of the 3PB device.

[1] SOLIDWORKS®, SolidWorks Corporation, Release 16

The study of the various configurations was accomplished by means of 3PB tests. Using an universal testing machine, namely Shimadzu AG-IS, as presented below in Figure 3.2 (a), along with the complete 3PB device. This testing machine is connected to a data acquisition software system, TRAPEZIUM[2], that allows the extraction of the experimental results. Finally, a Canon 5d mark III camera was used for the subsequent analysis of the angles produced by the laminated beams during the bending test, see Figure 3.2 (b).

(a) 3PB device coupled to the testing machine.

(b) Camera.

Figure 3.2: Instrumentation for the experimental practice.

[2]TRAPEZIUM®, Materials Testing Software, Shimadzu, Version 2

3.2 Laminated Beam Dimensioning

The present study relies on the analysis and test of a simply-supported laminated beam, under a concentrated force at its mid-span, as depicted in Figure 3.3. The laminated beam is composed by two layers, each one corresponding to a different material, and an interlayer (the adhesive). The total beam length and the distance between the supports were taken as L_t = 200 mm and L = 160 mm, respectively, and a beam width of b = 25 mm was chosen. H_a and H_b indicate the thickness of both layers, concerning the two different materials, respectively. H_t indicates the total thickness of the beam taking into account the adhesive layer. Moreover, since two adhesives of different nature were used, H_{tepoxy} and H_{tpecol} indicate the total thicknesses using epoxy resin and Pecol glue, respectively. These last two values were achieved by averaging the total thicknesses of three samples, considering each material configuration.

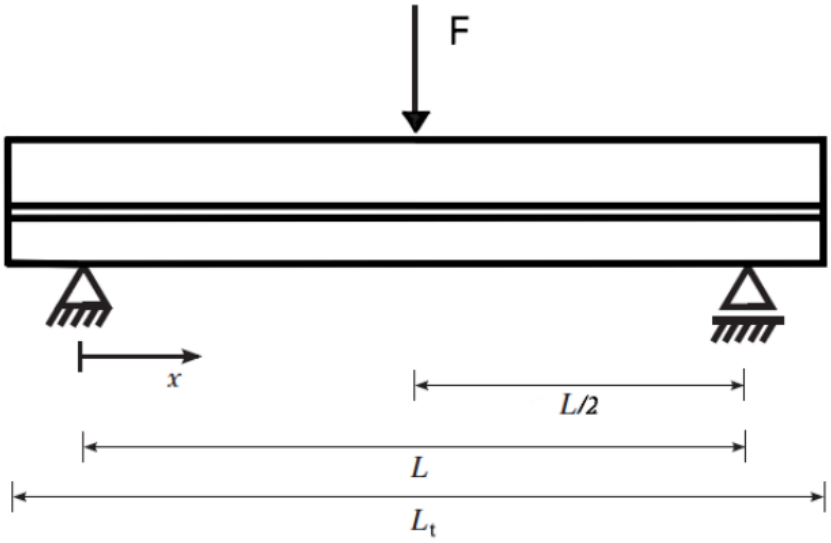

(a) Laminated beam model.

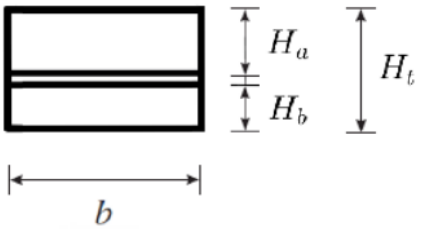

(b) Cross-section.

Figure 3.3: Simply-supported laminated beam and its cross-section geometry.

Assuming the purpose of combining different materials, Figure 3.4 presents a scheme of the three material configurations that were considered.

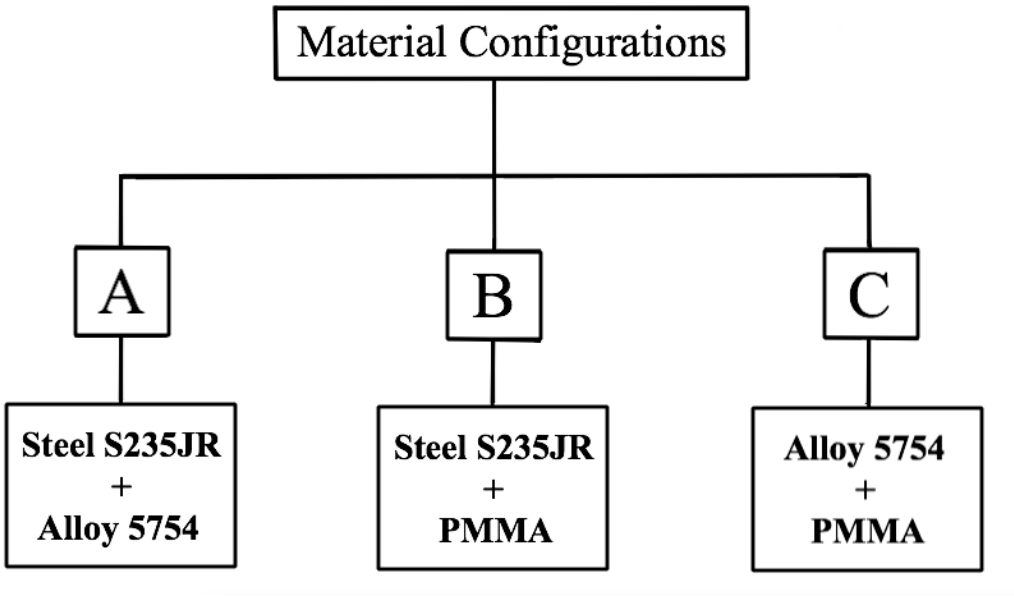

Figure 3.4: Diagram of material configurations studied.

In Table 3.1 are given the assigned values for the thicknesses mentioned above, concerning the three material configurations (A, B, C). The total bi-material beam thicknesses were measured with a calliper, whereas the thickness of each material, H_a and H_b were assumed to be the ones given in the material sheet given by the supplier. After bonding and through the same device, the total thickness of the beam taking into account the adhesive layer was registered, H_{tepoxy} and H_{tpecol}.

Table 3.1: Thicknesses of the laminated beam sets.

Material configuration	H_a [mm]	H_b [mm]	H_{tepoxy} [mm]	H_{tpecol} [mm]
A	3.00	5.00	8.11	8.41
B	3.00	5.00	8.15	8.41
C	5.00	5.00	10.16	10.41

3.3 Materials and their Properties

In a first experimental attempt, some 3PB tests were performed with some acquired samples. However, those samples were not enough to present repeatability of results. In section 3.5.2, more information will be detailed taking into account this factor. Therefore, it was decided that more samples had to be acquired to provide reliability in the final results. For this purpose, more samples were purchased, specifically samples made of Steel S235JR, Alloy 5754 and PMMA materials, as shown in Figure 3.5. These materials were chosen due to their distinct properties.

Figure 3.5: Different material samples used (before bonding).

In the same line of thought, it was decided to choose two different adhesives in order to investigate how they would affect the mechanical behaviour of the structure, as specified next.

The adopted adhesives were the Sicomin epoxy resin SR 1500 (with SD 2505 hardener) and the Pecol MSP 50 glue, as illustrated in Figure 3.6. On the one hand, epoxy resin is a thermoset, suitable for curing at room temperature. On the other hand, Pecol glue is an elastomer with drying time. In Appendices A.3 and A.4, more information is provided according to supplier catalogue tables.

(a) Epoxy resin.

(b) Pecol MSP 50.

Figure 3.6: Adhesives used for bonding.

The materials were not tested to obtain their mechanical properties. This work aims to have an insigth of using different materials and adhesives, using their nominal properties. It is known that for a more detailed study, the material properties of the bimaterial beams and their adhesives should be obtained by tests in controlled temperature and relative humidity conditions.

Table 3.2 gives the mechanical properties of the acquired materials, namely the Steel S235JR, the Alloy 5754 and the PMMA. Unfortunately, the supplier of the steel and aluminium samples could not provide the specifications catalogue. Therefore, their mechanical properties were obtained through [29]. Regarding the PMMA samples, acquired from a different supplier, the properties were taken from the obtained catalogue, presented in the Appendices A.5.

In Table 3.3 are presented the properties concerning each of both adhesives used. Due to the non-existence of the Poisson coefficient value for the Pecol adhesive, it was assumed as $\nu = 0.48$, which is the standard value for the rubber. This value was attributed given its elastic behaviour.

Table 3.2: Mechanical properties of the layers.

	Material layers		
Mechanical properties	**S235JR**	**Alloy 5754**	**PMMA**
Elastic modulus, E [GPa]	210	70	3.3
Shear modulus, G [GPa]	81	26	1.19
Yield strength, σ_y [MPa]	235	80	76
Ultimate tensile strength, σ_u [MPa]	360	210	76
Poisson coefficient, ν [-]	0.3	0.33	0.39
Mass density, ρ [kg/m^3]	7800	2660	1190

Table 3.3: Mechanical properties of each adhesive.

	Adhesive materials	
Mechanical properties	**Epoxy**	**Pecol**
Elastic modulus, E [MPa]	3000	0.9
Shear modulus, G [MPa]	1071.43	0.304
Poisson coefficient, ν [-]	0.4	0.48
Mass density, ρ [kg/m^3]	1200	1570

3.4 Simple 2D FE Model of the 3PB Beam

In this study, a 2D FE model of the three-point bending beam was developed in ANSYS[3], using plane 2D quadratic elements (solid Plane183), and assuming plane stress conditions.

The model considers three layers, namely, two layers representing the two different materials and a third one concerning the interlayer (adhesive). In addition, an applied concentrated force in the middle of the beam is considered to simulate the 3PB test adopted in this work. Due to the symmetry of the problem, only one half of the beam was considered in the analysis.

This simple FE model was made in order to help in the assessment of the necessary material thicknesses, to be used in the different configurations and respecting all the dimensions and machine load capacity (1 kN), in order to not surpassing the allowable stress limits of each material and respect other limitations in test device geometry, like span and width.

The first stage was to assume the geometrical properties according to the dimensions of the 3PB device. Depending on the material configuration, different mechanical properties should be defined: namely Young's modulus and Poisson's coefficient. Displacement and stress results are generated from the related configuration, such that it would be possible to get an idea of what could be the actual behaviour of the structure. In Figure 3.7 an overview of its mesh can be seen and in Figure 3.8 its Von Mises stress fringes are illustrated.

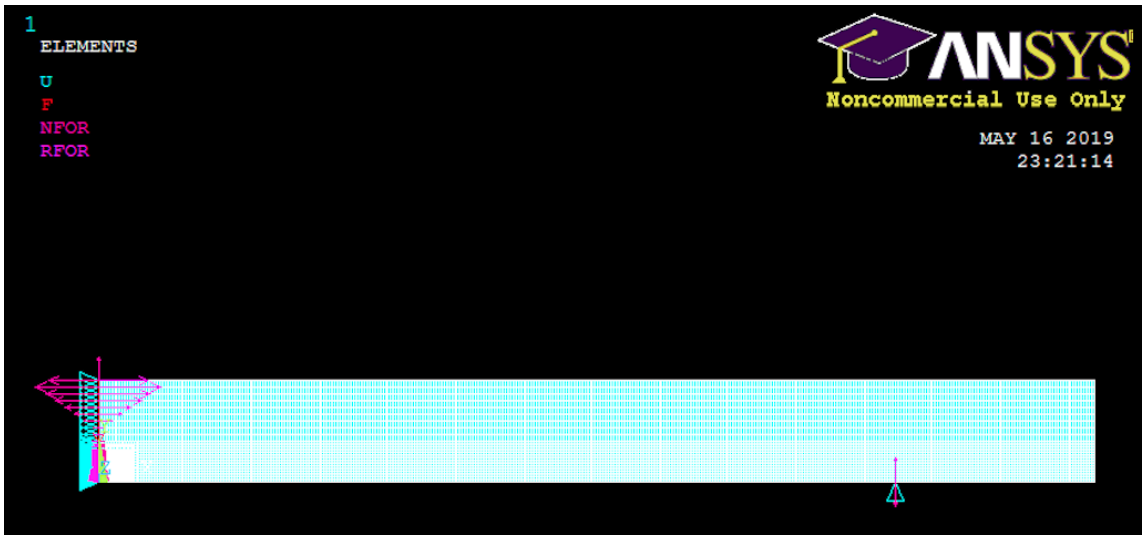

Figure 3.7: Laminated beam mesh.

[3]ANSYS® Academic Research Mechanical, Release 18.1

To achieve the optimum dimensions of the laminated composite beam, some conditions had to be satisfied. On one hand, it was imperative to ensure the final displacement values had to be significant within the elastic limits.

On the other hand, to ensure that the maximum Von-Mises stress was lower when compared to the maximum yield stress of the materials under test. This was possible after some manipulation between the estimated values (mechanical and geometric properties) and the generated values.

The approximate number of elements was 6090 elements and 18953 nodes.

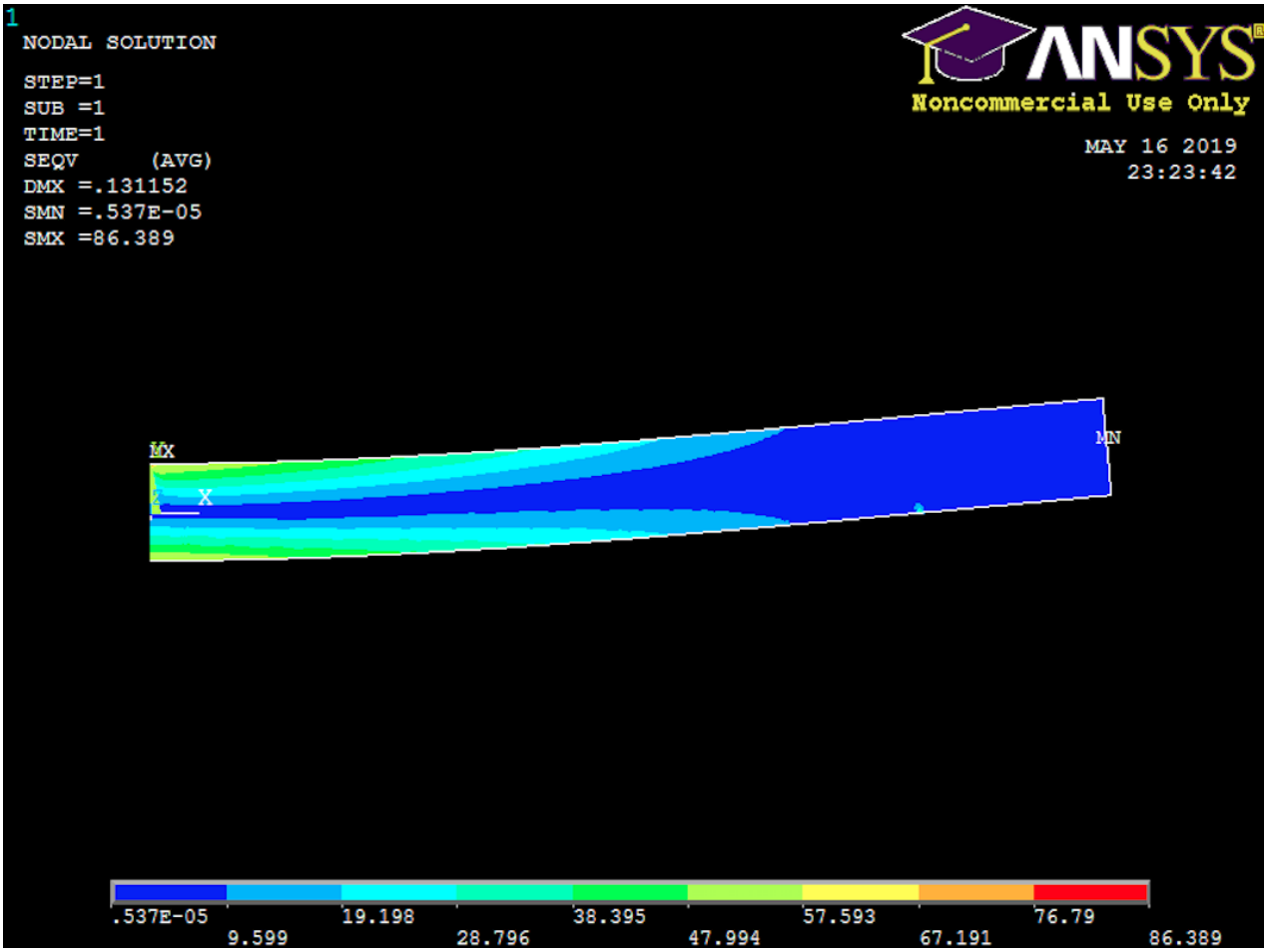

Figure 3.8: Von Mises stress fringes.

3.5 Three-Point Bending Test

3.5.1 Samples Preparation

Before starting the bending test itself, a whole preparation process was considered to obtain the specimens. This procedure is crucial since the better the bonding is, the more accurate the final experimental results will be.

After the samples acquisition, the surface cleaning stage and its bonding were performed. First, sandpaper was used to scratch the surface that would contact with the adhesive of all specimens, increasing roughness and thus a better penetration. Then, pure acetone was used to clean and to deoxidize the surfaces. This process was executed at every specimen to create a better adhesion between the two material layers.

(a) Creation of a rougher surface.

(b) Acetone and sandpaper used.

Figure 3.9: Samples preparation.

Subsequently, the materials were bonded using both types of adhesive, as mentioned before. This process requires extra care during its handling. On the one hand, there was the commitment that each surface would be fully covered with glue, avoiding air bubbles between the adhesive and the material layers. On the other hand, there was the need to carry out the process quickly, otherwise, the adhesive begins its curing process, that can lead to imperfections in the final result. This is noticeable especially in the thermoset epoxy, which has a faster cure time than Pecol adhesive.

Once the bonding process was finished the samples were placed between plates, and six configurations of each type were grouped with both adhesives so that the thickness was approximately the same and it would be possible to keep the plates horizontal. The cure of the beams was done with a set of weights for a period of one week, as illustrated in Figure 3.10.

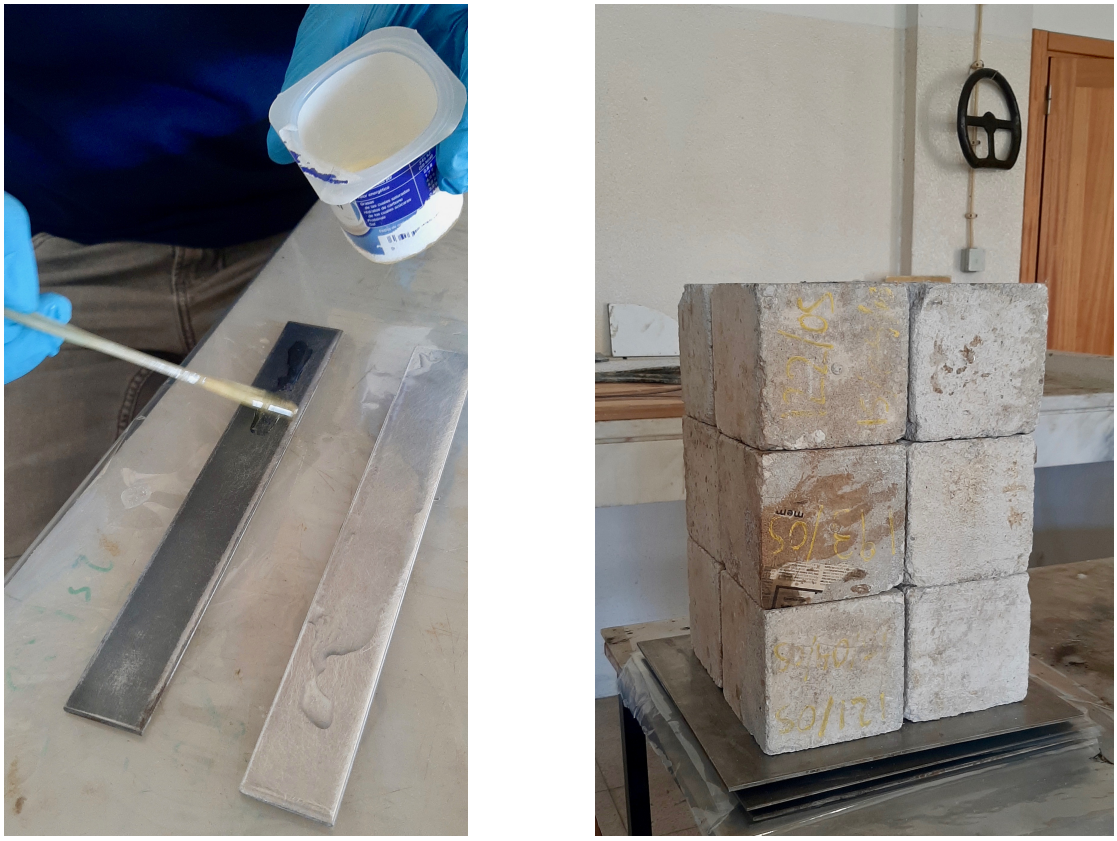

(a) Epoxy resin application.

(b) Compression by weights.

Figure 3.10: Bonding process.

3.5.2 Experimental Test

Following all the material acquisition and its arrangement, the 3PB tests were finally done, as depicted in Figure 3.11. The beam properties were inserted in the TRAPEZIUM software and the bending test was performed with a constant imposed displacement rate. The chosen test speed was 0,5 mm/min, the lowest possible value, to ensure the practice of a quasi-static regime since the numerical model does not take into account dynamic effects and also to minimize the non-linear viscous interaction of the adhesives. Although the desired results of this work are related to the linear elastic regime, the bending test was performed up to the plastic regime.

Figure 3.11: Laminated beam under a 3BP test.

3.5.3 Repeatability of Experiments

The repeatability of the experimental tests is important in this kind of studies since it contributes to a reduction in the uncertainty of the obtained results.

Moreover, the number of samples to be tested is relevant, in such a way that it is possible to obtain reliable results, taking into consideration each one of those samples for analysis.

Having said that, 36 material samples were obtained to perform a total of 18 bending tests. These numbers reflect three samples of each material configuration and were the possible obtained samples given the limited available resources.

Once the experimental practice begins, even if small, measurement errors will always be present. Here, repeatability of results is also a beneficial factor, since when there are several samples available for testing, it is possible to compare the obtained experimental results, which allows the minimization of the measurement errors.

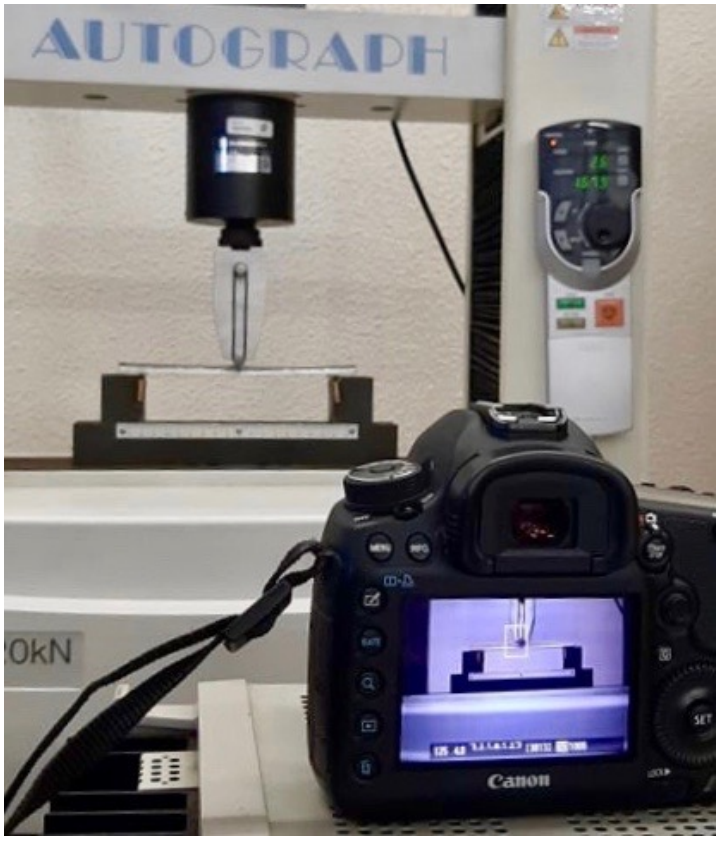

Figure 3.12: Experimental data aquisition.

Thus, two different types of errors can be highlighted: random errors and systematic errors.

A random error is related to the accuracy of the instrument, these are dependent on the considered instrument and can not be eliminated without the instrument change.

A systematic error is associated with human intervention. These errors are linked to imperfect experimental technique, which can either be related to experimental readings or imperfect instrument calibration. These types of errors can be decreased as the laboratory techniques of the analyst improve.

The accuracy of an experimental value is determined by the average value of multiple measurements, where x_i represents a measurement and n is the number of measurements.

$$average = \bar{x} = \frac{\sum_i x_i}{n} \tag{3.1}$$

The precision of a set of measurements can be determined by calculating the standard deviation for a set of data where $n - 1$ is the degrees of freedom of the system.

$$standard\ deviation = s = \sqrt{\frac{\sum_i (x_i - \bar{x})^2}{n - 1}} \tag{3.2}$$

Taking this information into consideration, the experimental results from the bending test performed on each of the material configurations will take into account these two factors mentioned above. The corresponding results and plots are presented and discussed in the following section.

Chapter 4

Results and Analysis

4.1 Numerical Analysis

4.1.1 Equilibrium FEM Model Approach

To obtain the numerical results, the equilibrium finite element model proposed in [2] is adopted to predict the structure behaviour. This model is based on a hybrid equilibrium-based finite element formulation for the static analysis of composite beams, in which the following mechanical assumptions are taken into account:

(i) Timoshenko assumptions are considered, which means that the shear effect is taken into account;

(ii) no uplift occurs between the two layers (i.e., both layers have the same transverse displacement);

(iii) slip can occur at the interlayer (i.e., partial interaction is assumed);

(iv) the material behaviour is linear elastic.

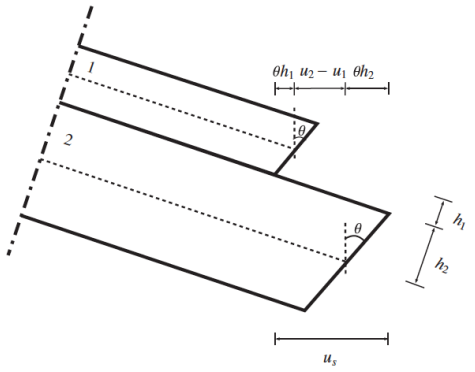

Figure 4.1: Interaction between the two-layers [2].

Unlike the conventional displacement models (FTOOLS, ABAQUS, ANSYS, etc), the equilibrium FEM model is an alternative model based on the approximation of the internal forces, bending moments and the interlayer shear force of the beam elements. This is in contrast with the conventional finite element models which relies on the approximation of the beam transverse displacement and rotation of the beam elements.

The approximations adopted in the equilibrium FEM model are chosen so that the equilibrium equations of the structural problem are strongly satisfied. More specifically, the approximations for the bending moments are taken as piecewise quadratic polynomials as follows [2]:

$$M_1^h = M_1^i \left(1 - \frac{x}{L}\right) + M_1^j \left(1 - \frac{x}{L}\right) - 4M_1^k \left(\frac{x(L-x)}{L^2}\right) \tag{4.1}$$

$$M_1^h = M_1^i \left(1 - \frac{x}{L}\right) + M_1^j \left(1 - \frac{x}{L}\right) - 4M_1^k \left(\frac{x(L-x)}{L^2}\right) \tag{4.2}$$

$$M_2^h = M_2^i \left(1 - \frac{x}{L}\right) + M_2^j \left(1 - \frac{x}{L}\right) - 4M_2^k \left(\frac{x(L-x)}{L^2}\right) \tag{4.3}$$

In which M_1^i, M_2^i and M_1^j, M_2^j are the bending moments of layers 1 and 2 at $x = 0$ and $x = L$, respectively and M_1^k and M_2^k are the mid-span bending moments of beams 1 and 2. The approximations for the shear and axial forces are [2]:

$$V^h = V_0 - qx \tag{4.4}$$

$$N_1^h = N_{10} + n_1 \left(\frac{x}{hL}\right) + n_2 \left(\frac{x^2}{hL^2}\right) \tag{4.5}$$

$$N_2^h = N_{20} + n_1 \left(\frac{x}{hL}\right) + n_2 \left(\frac{x^2}{hL^2}\right) \tag{4.6}$$

$$n_1 = M_1^j - M_1^i + M_2^j - M_2 i + 4\left(M_1^k + M_2^k\right) - V_0 L \tag{4.7}$$

$$n_2 = -4\left(M_1^k + M_2^k\right) + \frac{qL^2}{2} \tag{4.8}$$

In which V_0, N_{10} and N_{20} represent the shear force and axial force parameters defined at $x = 0$.

And q corresponds to the distributed load applied on the beam, which in the present case is $q = 0$.

In order to carry out the numerical simulations based on this FEM model, an already available MATHEMATICA[1] code was adopted, which makes use of a set of parameters as shown in Table 4.1.

Table 4.1: Parameters required for the numerical model.

Characteristics	**Designation**
H_a	Thickness of layer a
H_b	Thickness of layer b
b	Width of beam
E_a	Young's modulus of layer a
E_b	Young's modulus of layer b
G_a	Shear modulus of layer a
G_b	Shear modulus of layer b
L	Distance between the supports
k_s	Interlayer slip modulus
F	Applied force in the mid-span

Below are presented the response parameters that can be generated from the equilibrium model:
(i) Transverse and axial forces;
(ii) Interlayer shear force;
(iii) Relative axial displacement;
(iv) Bending moment;
(v) Transverse displacement;
(vi) Rotation angle.

[1]Wolfram Research, Inc., Mathematica, Version 11.3

To provide a better perception, Figures 4.2, 4.3, 4.4, 4.5, 4.6, 4.7, and 4.8 illustrate the results and plots provided by the numerical model. These figures in specific are related to the particular case of the material configuration B (Steel-PMMA), bonded with epoxy resin and with an applied force value of $F_{nom} = 300$ N. This nominal force value was chosen because it ensures that all material configurations are within the linear elastic regime.

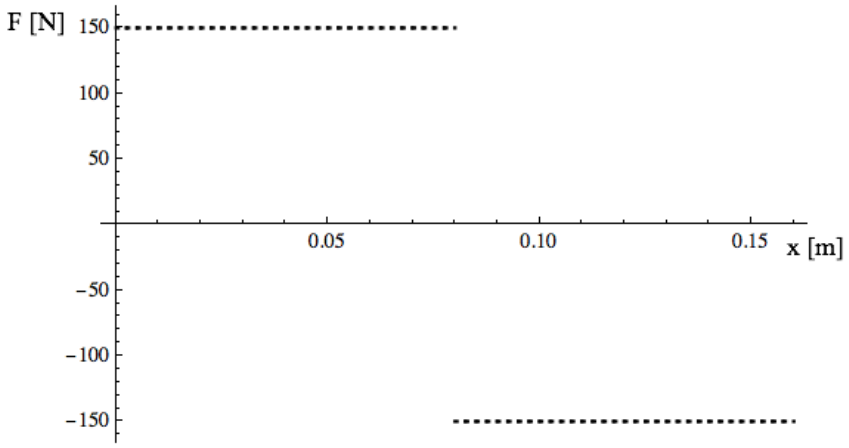

Figure 4.2: Transverse force.

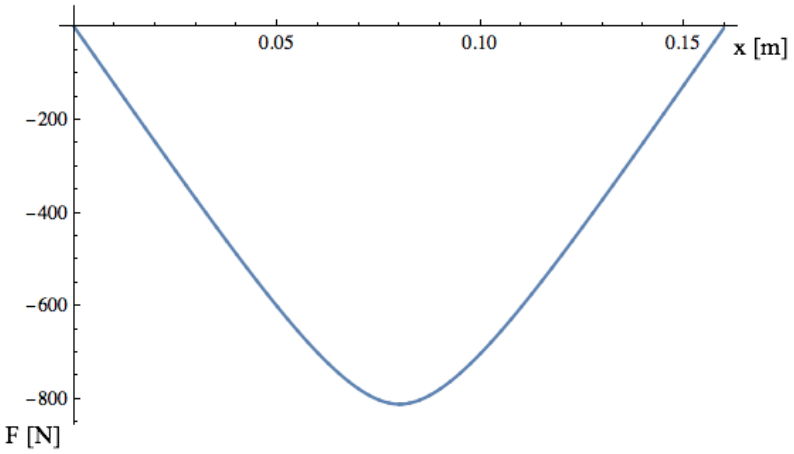

Figure 4.3: Axial force of layer a.

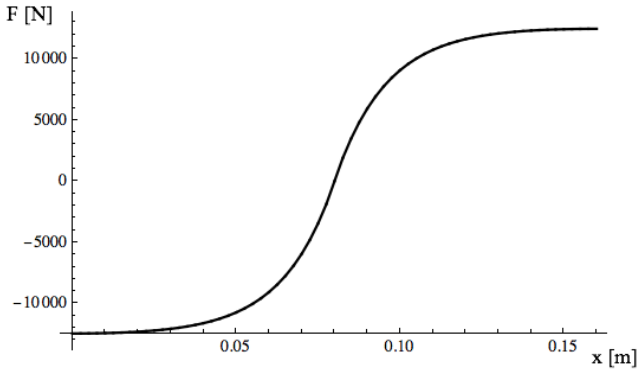

Figure 4.4: Interlayer shear force.

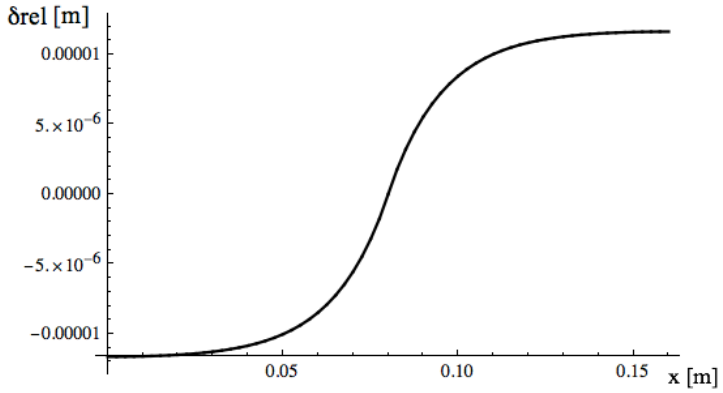

Figure 4.5: Relative axial displacement.

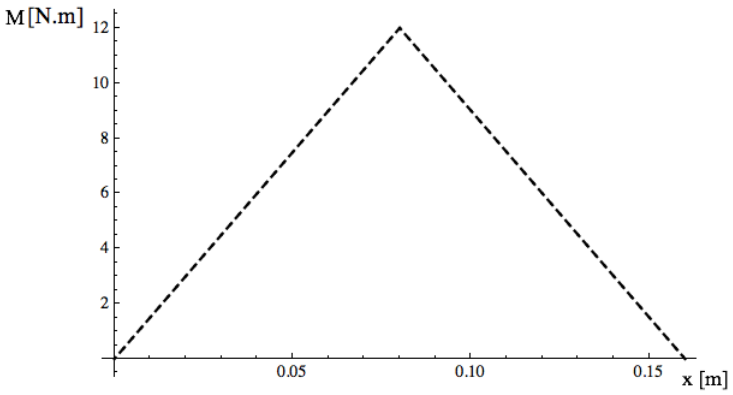

Figure 4.6: Bending moment.

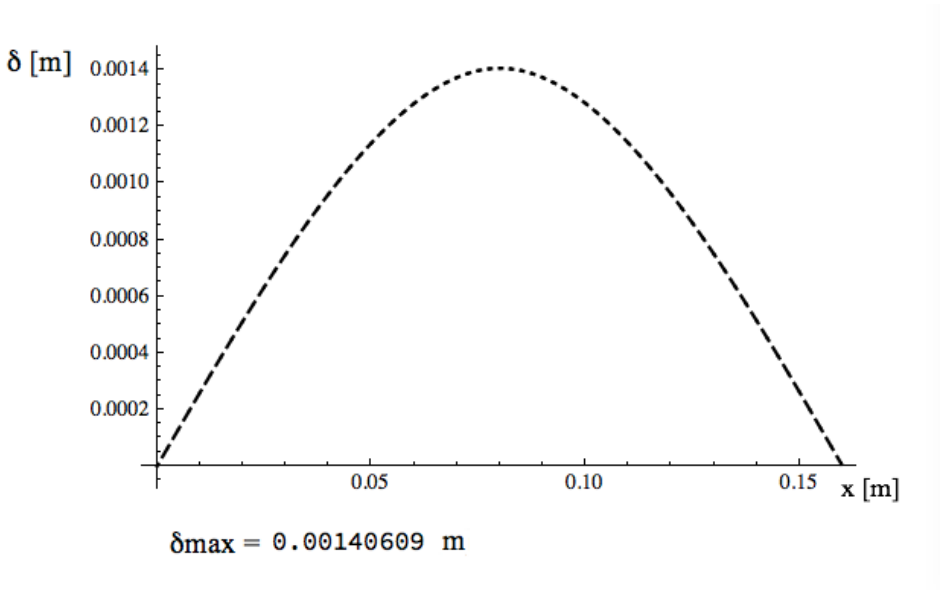

Figure 4.7: Deformed configuration of the beam and maximum transverse displacement.

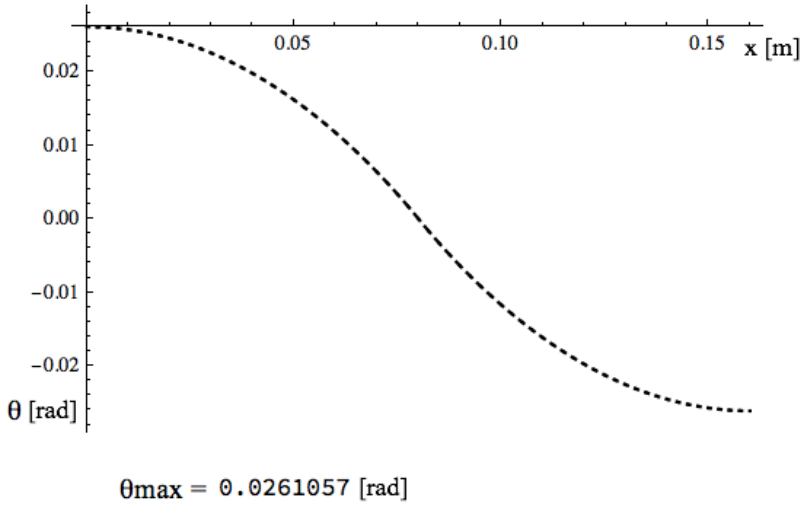

Figure 4.8: Rotation angle along the beam and maximum rotation angle in the edge of the beam.

Although the equilibrium FEM model can be used to obtain several response parameters, as mentioned above, only the maximum rotation angle and the maximum transverse displacement will be considered for this study, manifesting in this way the mechanical behaviour of the beam.

4.1.2 Equilibrium FEM Model Results

To obtain a coherent comparison between numerical and experimental methods, a nominal force value was considered, namely, $F_{nom} = 300$ N. Thus, considering the same value for the force in all cases, the corresponding results will be obtained and the comparison between the analysis methods will be carried out.

Besides the required mechanical parameters presented in the previous section, also the number of elements in which the beams are discretized is needed. In the present case, 64 finite elements were assumed in order to assure that accurate numerical results are obtained.

It should also be noted that in the present case, the parameter interlayer slip modulus, k_s, was considered as the shear modulus, G, of the adhesive.

Tables 4.2, 4.3 and 4.4 below show the results obtained by the numerical model, for each material configuration.

Table 4.2: Equilibrium model results for configuration A.

	F [N]	**Adhesive**	**Displacement δ** [mm]	**Rotation angle θ** [º]
Configuration A: Steel-Aluminium	100	Epoxy	0.145	0.172
		Pecol	0.289	0.286
	200	Epoxy	0.290	0.286
		Pecol	0.579	0.063
	300	Epoxy	0.434	0.458
		Pecol	0.868	0.917

Table 4.3: Equilibrium model results for configuration B.

	F [N]	Adhesive	Displacement δ [mm]	Rotation angle θ [º]
Configuration B: Steel-Polymer	100	Epoxy	0.468	0.515
		Pecol	0.674	0.745
	200	Epoxy	0.936	0.974
		Pecol	1.347	1.432
	300	Epoxy	1.404	1.489
		Pecol	2.021	2.177

Table 4.4: Equilibrium model results for configuration C.

	F [N]	Adhesive	Displacement δ [mm]	Rotation angle θ [º]
Configuration C: Aluminium-Polymer	100	Epoxy	0.316	0.344
		Pecol	0.461	0.516
	200	Epoxy	0.632	0.687
		Pecol	0.921	0.974
	300	Epoxy	0.948	1.031
		Pecol	1.382	1.489

4.2 Experimental Analysis

4.2.1 Three-Point Bending Test Results

This section exposes the obtained experimental results for the three material configurations A, B and C.

To accomplish further comparison between experimental and numerical results, detailed in section 4.3, all the values presented in Table 4.5 refer to the nominal force value $F_{nom} = 300$ N. The experimental results were achieved through some mathematical manipulation, specifically through some linear interpolation for the adopted nominal force value and, subsequently, by averaging the obtained results of the samples. The results are followed by their standard deviations (SD).

Table 4.5: Experimental results considering each adhesive.

Config.	**Adhesive**	**Displacement δ** [mm]	SD_δ [mm]	**Rotation angle θ** [º]	SD_θ [º]
A	Epoxy	0.275	0.017	0.567	0.201
	Pecol	0.908	0.035	1.274	0.009
B	Epoxy	1.628	0.031	1.692	0.203
	Pecol	1.979	0.074	2.057	0.147
C	Epoxy	1.308	0.226	1.306	0.334
	Pecol	1.364	0.104	1.460	0.133

The experimental displacement values were generated directly through the TRAPEZIUM software, as when a bending test is started, a real-time graph of the applied force as a function of displacement is generated.

In contrast, the rotation angle values were achieved afterwards through an additional software, named IMAGEJ[2]. With the support of time, force and displacement values, it was possible to select which photo corresponded to a certain applied force value. Then, with the angle command of IMAGEJ software, the beam rotation value was measured, as is illustrated in Figure 4.9.

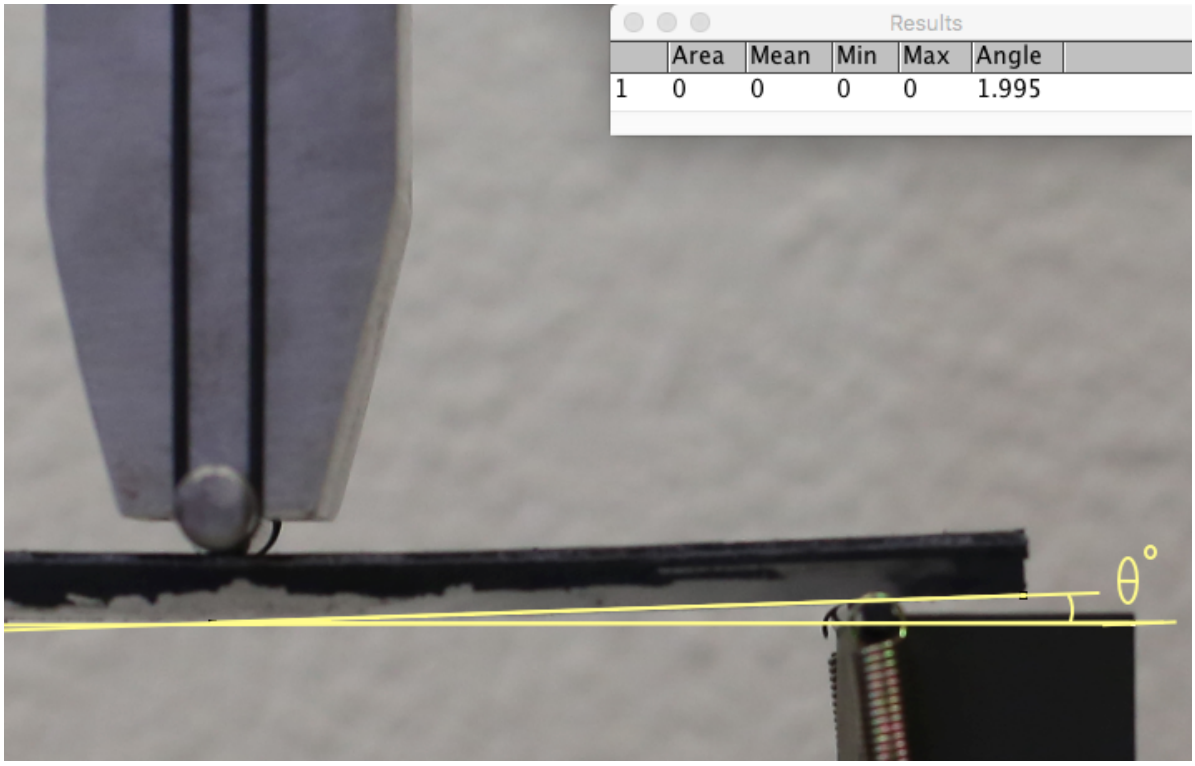

Figure 4.9: Rotation angle calculation.

[2]Rasband, W.S., ImageJ, U. S. National Institutes of Health, Bethesda, Maryland, USA.

4.2.2 Applied Force Vs Displacement Plots

The plots of the applied force versus displacement produced, concerning each material configuration tested, are presented below. The plots present the load-displacement curves of both adhesives. The lines are identified with the standard deviations as well, reflecting the three existing samples for each specific case.

Configuration A is the case in which the difference between the slopes of the two straight lines is more evident, with the slope of the epoxy adhesive being three times higher than the slope of the Pecol adhesive. Since this is the most rigid configuration, this is the case where the difference between using the resin and an elastomer is found.

Being this the most toughness configuration when compared with the other two, it was the one that presented the highest values of applied force before reaching plasticity. However, the one with Pecol adhesive achieved higher displacements values before reaching plasticity.

Note that, as expected, the standard deviation increase with load. In this particular configuration, small deviations are observed.

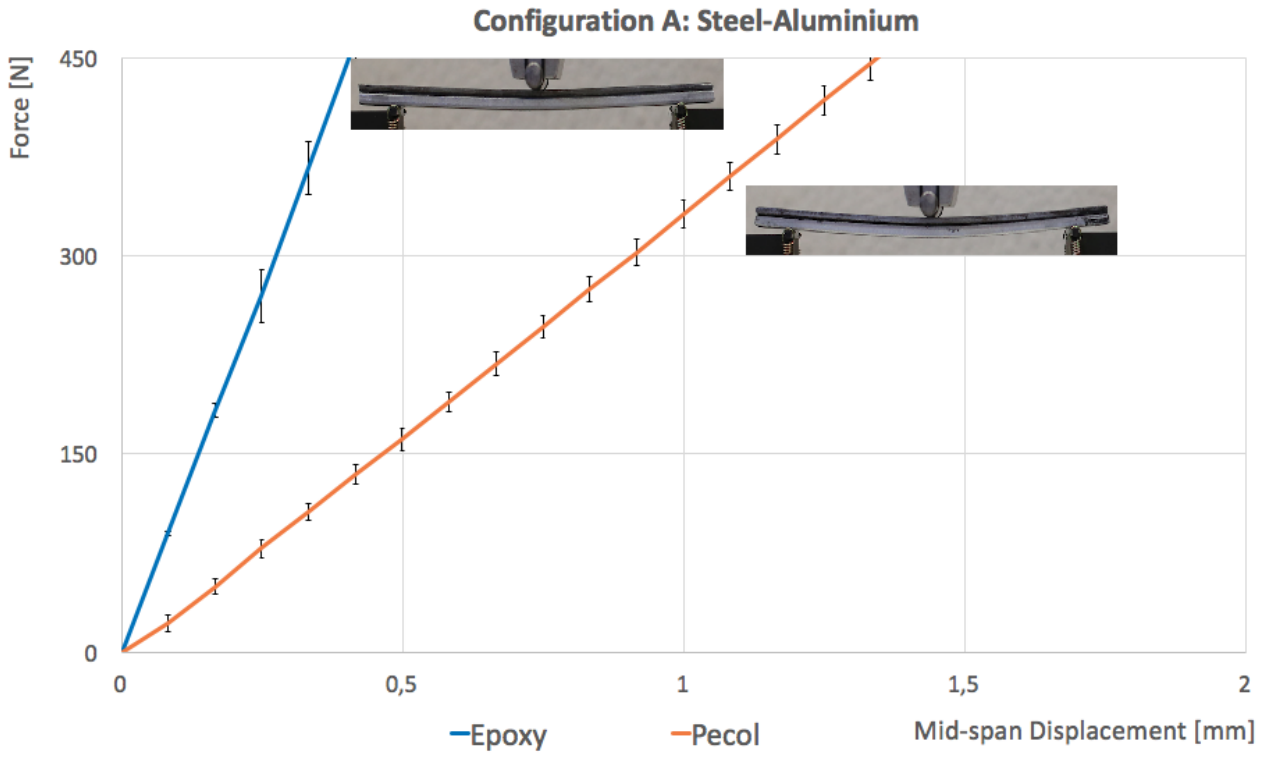

Figure 4.10: Applied force Vs Displacement produced in configuration A for both adhesives.

Concerning configuration B, it is possible to verify a more similar behaviour exhibited by both adhesives, although the epoxy resin being always the adhesive that contributes to a final higher configuration stiffness. In respect to the standard deviations, considering the three samples, minimal values were obtained. It should also be noted that in configuration B, made up of Steel + PMMA, present a higher relative displacement when compared to what happens in configurations A and C. Likewise, this configuration also presented the highest verified value of the angle produced at the end of the beam.

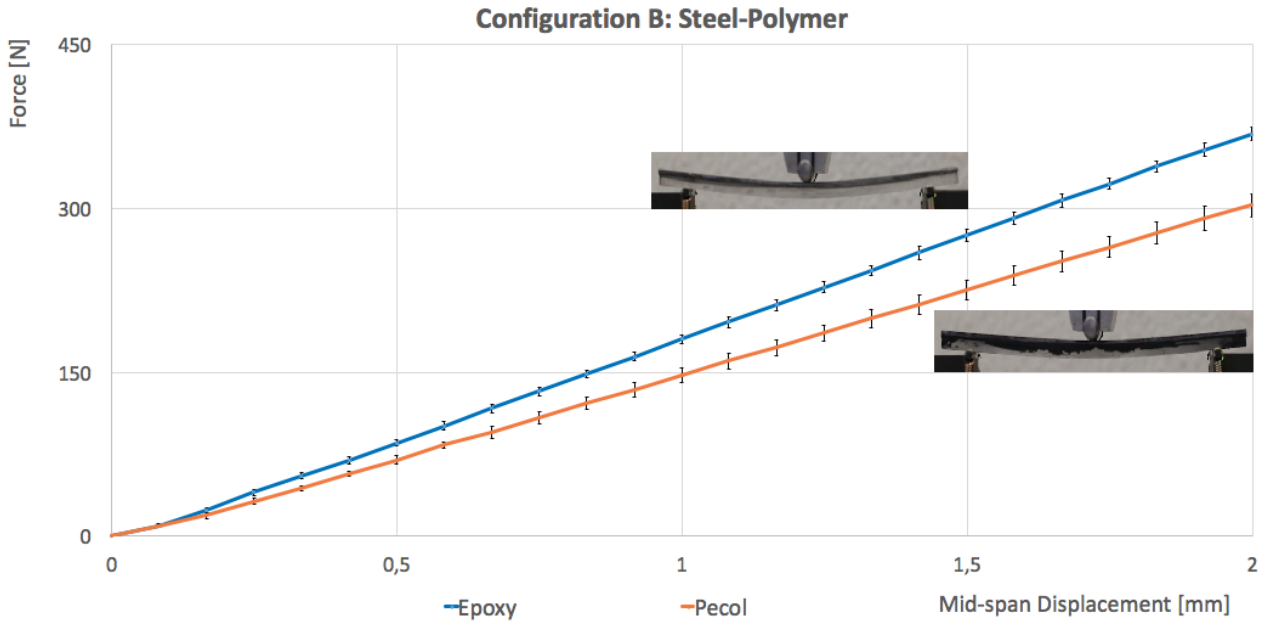

Figure 4.11: Applied force Vs Displacement produced in configuration B for both adhesives.

Regarding configuration C, see Figure 4.12, both lines present the highest standard deviation when compared to configurations A and B, also noticeable in Table 4.5. One possible reason for this discrepancy can be related to the load cell reading of the testing machine. In other words, when placing a sample in the testing machine, there is the need to manually adjust the upper part of the bending device so that it remains on the verge of contact with the beam.

Since configuration C was the first to be tested, subsequently, when testing samples of configurations A and B, a greater care was taken with this detail, which led to more accurate results. Besides that, it can be seen a sligth non-linearity at the beginning, possible atributted to PMMA.

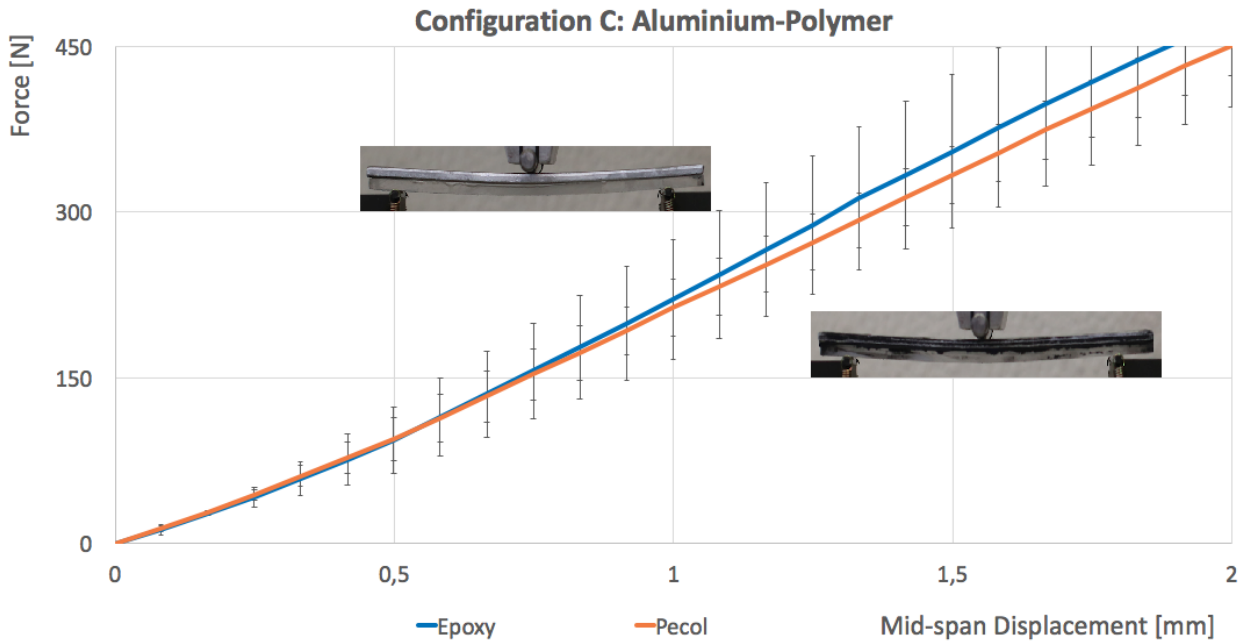

Figure 4.12: Applied force Vs Displacement produced in configuration C for both adhesives.

It is interesting how different values were obtained in all cases. This fact reinforces the idea of how significant is the choice of materials depending on the purpose for which a particular structure is designed. In the following section, the numerical method results are compared with the obtained experimental results and, also, the relative errors between each method are presented and discussed.

4.3 Comparative Analysis of Results

In Table 4.6 are presented the relative errors of displacement ($\boldsymbol{\delta}$) and rotation angle ($\boldsymbol{\theta}$), respectively. These values are related to the numerical and experimental results, concerning the mechanical behaviour of the laminated beams, as presented in the previous sections 4.1.2 and 4.2.1. Thus, the values presented refer to the nominal force value $F_{nom} = 300$ N. Again, this is the value of which all the material configurations manifest their behaviour within the linear elastic regime.

Figures 4.13, 4.14 and 4.15 indicate the plots of the displacement produced by each analysis method, as well as each material configuration and adhesive used.

In this section, it was decided to illustrate only the plots related to the displacement produced since the rotation angle response is directly associated.

Table 4.6: Relative errors of the displacement and rotation angle obtained.

Config.	**Adhesive**	$\boldsymbol{\delta}$ **Relative Error** [%]	$\boldsymbol{\theta}$ **Relative Error** [%]
A	Epoxy	58.18	23.80
	Pecol	4.41	38.93
B	Epoxy	13.76	13.63
	Pecol	2.12	5.83
C	Epoxy	27.52	26.67
	Pecol	1.32	2.13

Regarding the displacement relative errors in Table 4.6, the value that stands out compared to all the others is the relative error value of 58.18%, obtained in configuration A when using epoxy resin as adhesive. In a second analysis, it is apparent that the relative error in the configurations using epoxy is always higher when compared to the Pecol adhesive. Despite the high error for the epoxy resin, the obtained results for the Pecol adhesive present a good correlation.

Since the experimental results are real values, they are assumed as defaults. The numerical results, on the other hand, are exclusively obtained from the required parameters assumed. Thus, the error obtained is justified by the lack of control in the parametric mechanical values introduced in the numerical model. Assuming that the mechanical properties of the material layers are correct, the error issue is related to the interlayer slip modulus that was adopted.

Although the values indicated in the adhesive catalogue were considered, several factors might have influenced this error, as will be discussed in the following paragraphs.

It should be noted that a scale has been used to satisfy the requirements for the specific quantities to be assumed when mixing resin and hardener, namely 33% of the total weight of the mixture should be hardener.

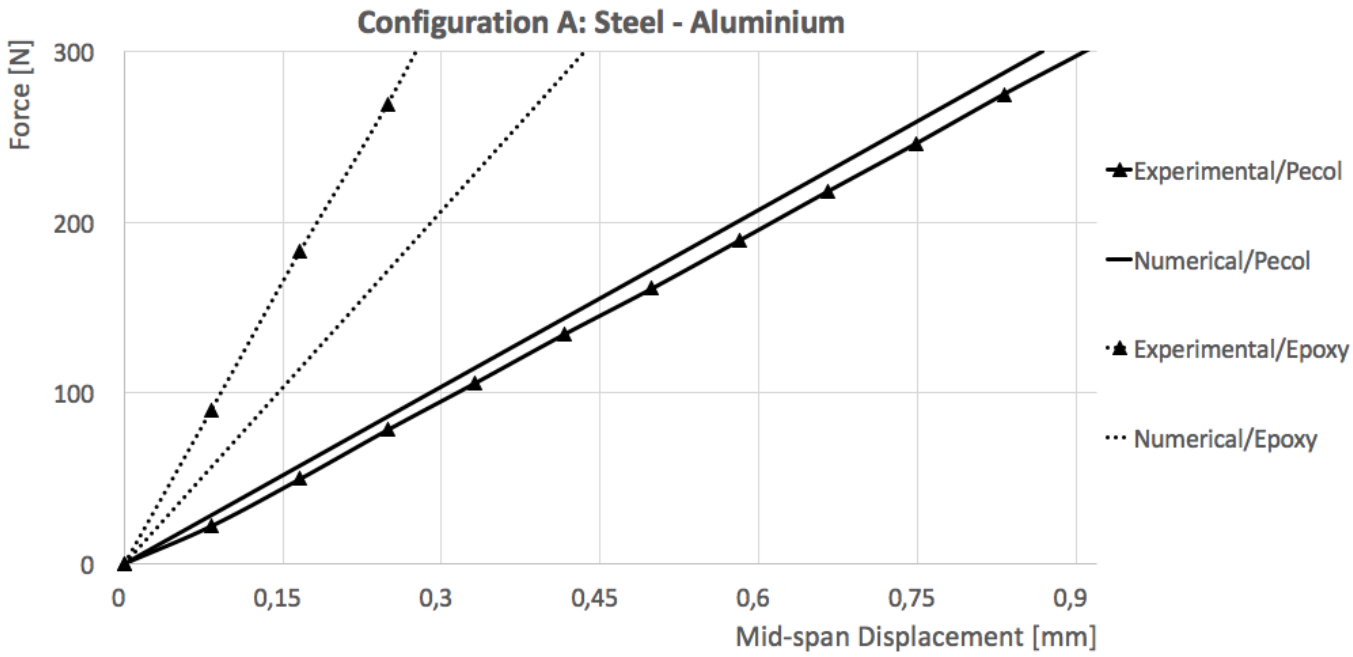

Figure 4.13: Comparative displacement results of configuration A.

Another reason is related to the laminated beams cure after bonding. During the curing week, the samples remained in a place where the ambient temperature was a little high, as this procedure was carried out in mid-August. This could also be a possible factor that has affected the assumed value, as the given values by the supplier refer to a cure in a 23° C atmosphere.

To prevent such a phenomenon, bonding would require special conditions. For example, the use of a controlled atmosphere by using vacuum aid, thus, no drastic changes in the mechanical properties of the resin would happeen.

In the case of configuration B, it can be seen that the difference between both methods of analysis remains slightly high when using epoxy resin. However, the results using Pecol adhesive, managed by both analysis methods are very consistent, see Figure 4.14. Such fact reinforces that there is a good behaviour prediction by the numerical model and that the error presented for the cases bound by epoxy resin is related to the assumed properties.

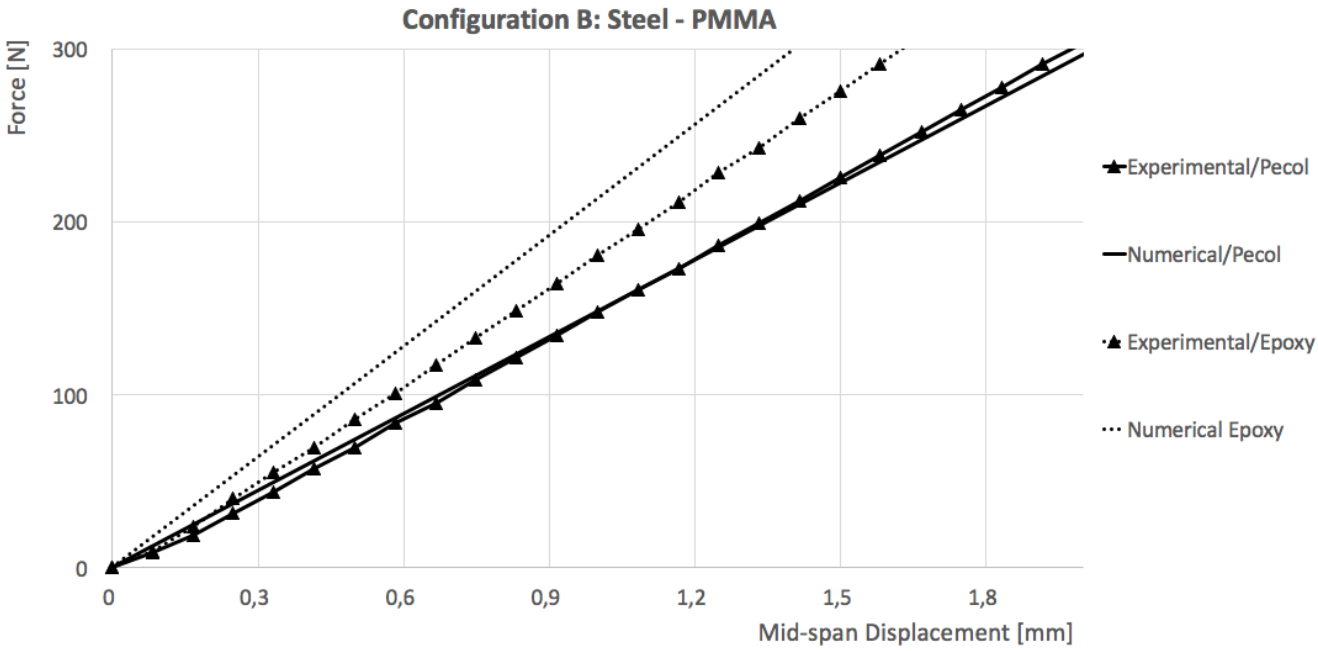

Figure 4.14: Comparative displacement results of configuration B.

Regarding the material configuration C, the relative error increases again, considering the epoxy resin bound case. On the other hand, despite the issues faced with the test machine load cell, this was the case that presented the smallest relative error when using Pecol glue, leading to a difference of nearly 1% between both methods.

Although some considerable errors were obtained, the numerical and experimental methods were successfully compared, as registered cases showed errors under 5%.

The disparity between the results that were bonded through the epoxy resin is most likely due to the distortion modulus value assumed for the interlayer in the numerical model.

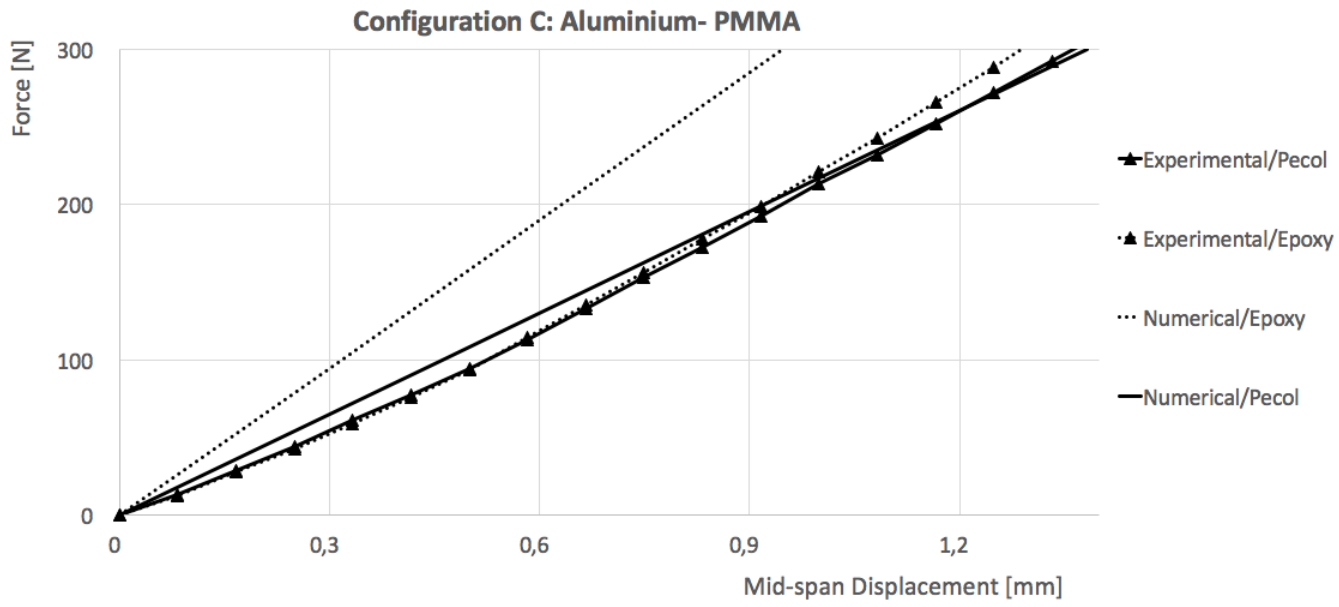

Figure 4.15: Comparative displacement results of configuration C.

Chapter 5

Conclusions

The present dissertation comprised the study of laminated composite beams bonded by two different types of adhesives, analyzing their mechanical behaviour through numerical and experimental analysis.

Samples of three different materials were used and three different configurations were subsequently studied, namely Steel-Aluminum, Steel-PMMA and Aluminum-PMMA, designated by configuration A, B and C, respectively. Regarding the adhesives, two different types were used, namely epoxy resin and Pecol sealant glue. A total of three samples were obtained for each specific configuration/adhesive case in order to assure repeatability.

Regarding the numerical modelling, an equilibrium FEM model was also used, whose inputs were the materials geometry and mechanical properties of layers and adhesives and after solving the equilibrium equations, enabled the retrievement of transverse displacements and rotation angles of the beams.

Moreover, an experimental investigation was performed to validate the results obtained by numerical predictions. Some discrepancies have been observed in particular in the case of the samples with epoxy adhesive.

Given the work described in this dissertation, the following conclusions may be formulated:

- The configurations bonded with the Pecol adhesive presented results obtained experimentally very close to the results obtained numerically, namely with a relative error from nearly 1% up to 4%. Such fact indicates that the finite element numerical model in question produces solutions close to reality;

- The errors obtained from the material configurations connected by epoxy resin were evidenced due to the lack of control in the values assumed by the numerical model, especially of its mechanical parameters (epoxy distortion modulus). Therefore, it would not be suitable to state an incoherent prediction by the numerical model, since the problem concerns the input data;

- The results obtained by Ansys 2D model are not presented, as they did not provide such a good correlation, so it would be a promising subject to improve in the future;

- The careful choice and preparation of the adhesives are very important when designing a laminated composite beam. This was evident in this work due to several reasons, such as the atmosphere and the surrounding temperature during the bonding process. If the adhesive requires mixing of resin and hardener, as was the case with epoxy resin, meticulously measure the resin and hardener amount and reduce to the maximum the creation of air bubbles by making a previous degassing of the prepared resin container.

Chapter 6

Future Developments

In order to give continuation to the study developed during the preparation of this dissertation, the following suggestions for possible future developments are presented:

- Improve the present 2D Ansys model, investigating the effect of using more than one element in thickness. Study the effect of plane stress and strain;

- Consider a 3D Ansys model for analysis;

- Consider a more effective method of acquiring images of the blade distortion using a higher magnification camera or microscope and capture frontal images. Improve the measuring technique of displacement and also read the strain in the bottom and eventually top layers (using strain gauges). Consider also the use of Digital Image Correlation (DIC);

- Extend the present study to a different range analysis. Explore different analysis regimes, entering the plastic domain and considering the fracture process between the adhesive and layers;

- Construct other batch of configurations with more specimens and more exaustive measurements in thickness in several locations;

- Further investigate the experimental evaluation of the epoxy resin elastic modulus;

- Perform mechanical testing to all the materials in order to mitigate possible errors atributted to their mechanical properties;

- Adopt more than two layers with different geometries. In such way, analyze the differences and similarities and the advantages/disadvantages of each structure/geometry;

- Adopt different boundary and support conditions.

Bibliography

[1] R.M. Jones. Mechanics of composite materials. *Tayler and Francis*, Second edition: 37–60, 1998.

[2] H.A.F.A. Santos and V.V. Silberschmidt. Hybrid equilibrium finite element formulation for composite beams with partial interaction. *Composite Structures*, 108: 646–656, 2014.

[3] Madreperla: Cast Acrylic Sheets. `http://files.plexicril.pt/200000241-73c6c74c0d/Madreperla%20Polarlite%20Data%20Sheet.pdf`

[4] E. Carrera, G. Giunta, and M. Petrolo. Beam Structures: Classical and Advanced Theories. *Wiley*, First edition: 9–22, 2011.

[5] N.M. Newmark, C.P. Siess and I.M. Viest. Tests and analysis of composite beams with incomplete interaction. *Proc. Soc. Exp. Stress Anal*. 9 (1): 75–92, 1951.

[6] J. Goodman and E. Popov. Layered beam system with inter-layer slip. *J Struct*, Division ASCE 94(11): 2537–2547, 1968.

[7] U.A. Girhammar and V.K.A. Gopu. Composite beam-columns with interlayer slip-exact analysis. *Journal of Structural Engineering*, ASCE 119 (4): 1265–1282, 1993.

[8] Y.C. Wang. Deflection of steel–concrete composite beams with partial shear interaction. *Journal of Structural Engineering*, ASCE 124 (10): 1159–1165, 1998.

[9] Y.F. Wu, D.J. Oehlers and M.C. Griffith. Partial-interaction analysis of composite beam/column members. *Mechanics of Structures and Machines*, 30 (3): 309–332, 2002.

[10] J.B.M. Sousa and A.R. da Silva. Analytical and numerical analysis of multilayered beams with interlayer slip. *Engineering Structures*, 32: 1671–1680, 2010.

[11] V. Adámek. The limits of Timoshenko beam theory applied to impact problems of layered beams. *International Journal of Mechanical Sciences*, 145: 128–137, 2018.

[12] M.J. Smyczynski and E. Magnucka-Blandzi. The three-point bending of a sandwich beam with two binding layers – Comparison of two nonlinear hypotheses. *Composite Structures*, 183: 96–102, 2018.

[13] F. Campi and I. Monetto. Analytical solutions of two-layer beams with interlayer slip and bi-linear interface law. *International Journal of Solids and Structures*, 50: 687–698, 2013.

[14] M.F. Domínguez. Modeling of the Bending Stiffness of a Bimaterial Beam by the Approximation of One-Dimensional of Laminated Theory. 4:6, 2014.

[15] H. Arvin and F. Bakhtiari-Nejad. Nonlinear free vibration analysis of rotating composite Timoshenko beams. *Composite Structures*, 96: 29–43, 2013.

[16] S. Schnabl, M. Saje and G. Turk, I. Planinc. Analytical solution of two-layer beam taking into account interlayer slip and shear deformation. *Journal of Structural Engineering*, 133(6): 886–894, 2007.

[17] Q.H. Nguyen, E. Martinelli and M. Hjiaj. Derivation of the exact stiffness matrix for a two-layer Timoshenko beam element with partial interaction. *Engineering Structures*, 33 (2): 298–307, 2011.

[18] R. Wu and Y. Wu. Static, dynamic, and buckling analysis of partial interaction composite members using Timoshenko's beam theory. *International Journal of Mechanical Sciences*, 49 (10): 1139–1155, 2007.

[19] A. Cernescu and J. Romanoff. Bending deflection of sandwich beams considering local effect of concentrated force. *Composite Structures*, 134: 169–175, 2015.

[20] I. Ecsedi and A. Baksa. Static analysis of composite beams with weak shear connection. *Applied Mathematical Modelling*, 35: 1739–1750, 2011.

[21] H. Murakami. A Laminated beam theory with interlayer slip. *Journal of Applied Mechanics*, 551–559, 1984.

[22] E. Martinelli, C. Faella and G. di Palma. Shear-flexible steel–concrete composite beams in partial interaction: closed-form "exact" expression of the stiffness matrix. *Journal of Structural Engineering*, 151–163, 2012.

[23] P. Le Grognec, Nguyen and M. Hjiaj. Exact buckling solution for two-layer Timoshenko beams with interlayer slip. *International Journal of Solids and Structures*, 49: 143–150, 2012.

[24] M. Avalle , L. Peroni , M. Peroni and A. Scattina. Bi-Material Joining for Car Body Structures: Experimental and Numerical Analysis *The Journal of Adhesion*, 86: 5-6, 539-560.

[25] T. Carlberger and U. Stigh. Dynamic testing and simulation of hybrid joined bi-material beam. *Thin-Walled Structures*, 48: 609–619, 2010.

[26] Z. Li, J. Zhao, F. Jia, Q. Zhang, X. Liang, S. Jiao, and Z. Jiang. Analysis of bending characteristics of bimetal steel composite. *International Journal of Mechanical Sciences*, 148: 272–283, 2018.

[27] P. Paczos, R. Wichniarek, and K. Magnucki. Three-point bending of sandwich beam with special structure of the core. *Composite Structures*, 201: 676–682, 2018.

[28] J.B. Sauvage, M. Aufray, J.P. Jeandrau, P. Chalandon, D. Poquillon, and M. Nardin. Using the 3-point bending method to study failure initiation in epoxide-aluminum joints. *International Journal of Adhesion and Adhesives*, 75: 181–189, 2017.

[29] Automation Creations, Inc. MatWeb, Your Source for Materials Information. `http://www.matweb.com/. Retrieved at April 16, 2009, from the website temoa : Open Educational Resources (OER) Portal at http://temoa.tec.mx/node/17168.`

Appendix A

Attachments

A.1 Steel composition for the upper part of the 3PB device

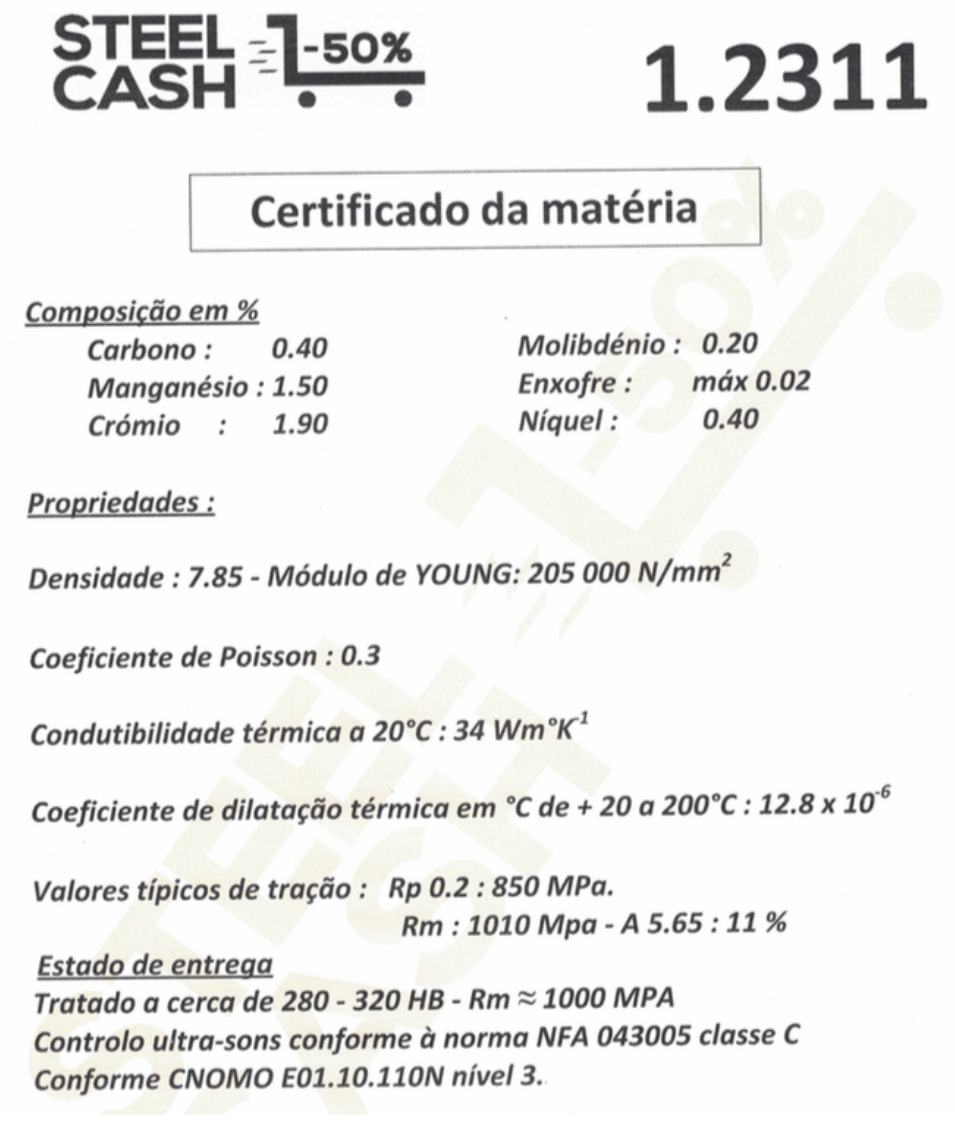

STEEL CASH -50%

1.2311

Certificado da matéria

Composição em %

Carbono :	0.40	Molibdénio :	0.20
Manganésio :	1.50	Enxofre :	máx 0.02
Crómio :	1.90	Níquel :	0.40

Propriedades :

Densidade : 7.85 - Módulo de YOUNG: 205 000 N/mm^2

Coeficiente de Poisson : 0.3

Condutibilidade térmica a 20°C : 34 $Wm°K^{-1}$

Coeficiente de dilatação térmica em °C de + 20 a 200°C : 12.8 x 10^{-6}

Valores típicos de tração : Rp 0.2 : 850 MPa.
Rm : 1010 Mpa - A 5.65 : 11 %

Estado de entrega

Tratado a cerca de 280 - 320 HB - Rm ≈ 1000 MPA
Controlo ultra-sons conforme à norma NFA 043005 classe C
Conforme CNOMO E01.10.110N nível 3.

A.2 Upper part of the 3PB device dimensioning

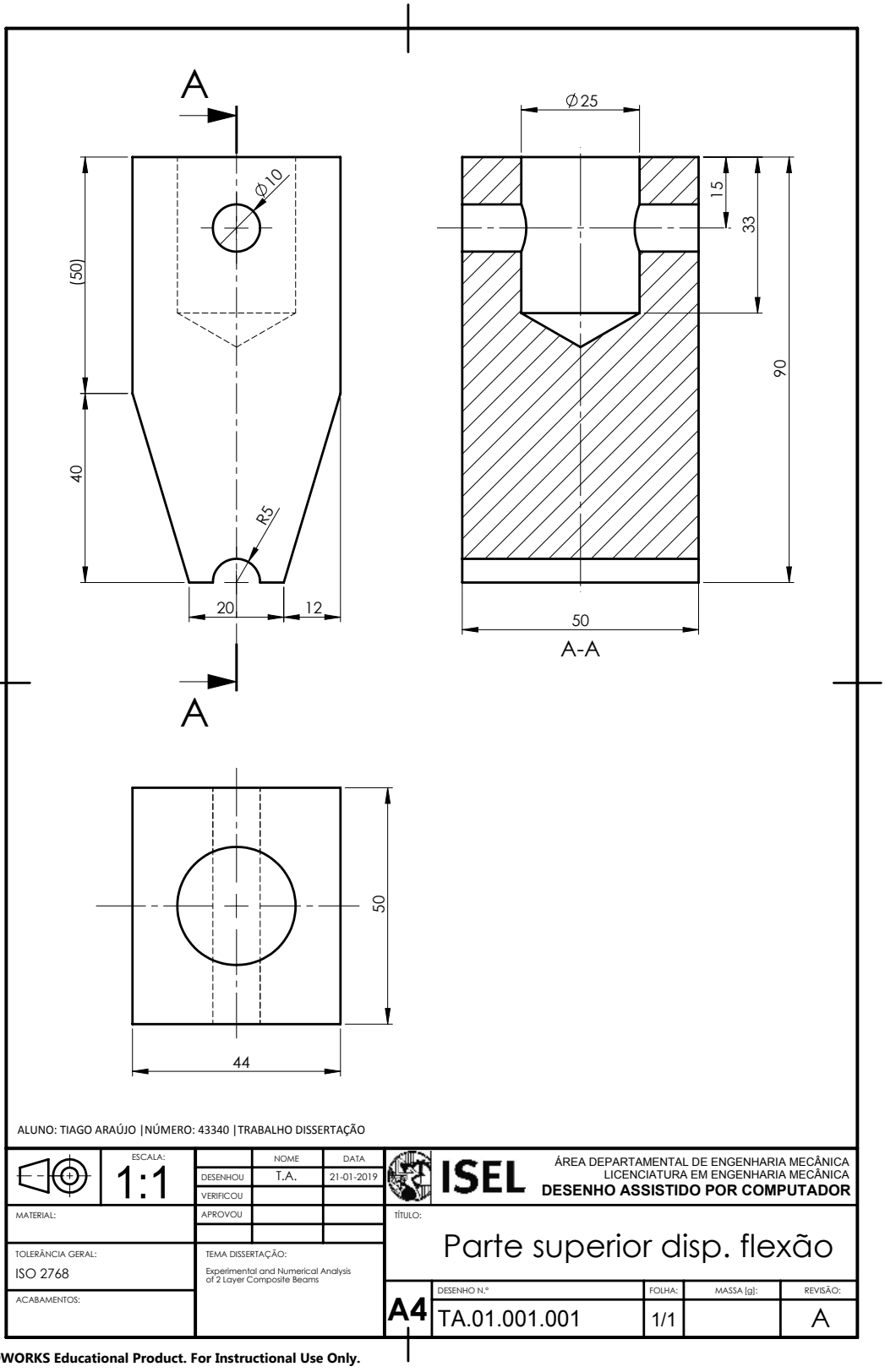

A.3 Epoxy resin specs

Sicomin Epoxy Systems TECHNICAL DATASHEET

Mechanical properties on pure cast :

		SR 1500 / SD 2505		
Curing cycles		14 jours 23 °C	24 h 23°C + 24h 40°C	24 h 23°C + 8h 60 °C
Tension				
Modulus of elasticity	N/mm^2	3100	2900	2900
Maximum resistance	N/mm^2	77	74	74
Resistance at break	N/mm^2	71	68	68
Elongation at max. load	%	3.6	4.4	4.7
Elongation at break	%	4.5	6.0	7.4
Flexion				
Modulus of elasticity	N/mm^2	3200	3100	3100
Maximum resistance	N/mm^2	115	115	117
Elongation at max. load	%	4.8	5.4	5.6
Elongation at break	%	7.7	8	7.9
Charpy impact strength				
Resilience	kJ/m^2	25	30	26
Glass Transition / DSC				
Tg1	°C	56	68	72
Tg1 max.	°C			76

A.4 Pecol MSP 50 specs

PECOL® Vedação e Colagem Selante

MSP 50 **Special**

Dados técnicos

Tipo de Selante	Híbrido com polímeros silano-terminados
Cor	Branco, cinza e outras sob consulta
Consistência	Pastosa

	UNIDADE	NORMA	VALOR
Densidade a +23°C	g/cm³	DIN	1,57
Tempo de formação de película (+23°C / 50%HR)	min	DIN 50014	15-30
Velocidade de polimerização (+23°C / 50%HR)	mm/dia	DIN 50014	2,5
Contração de volume	%	DIN 52451	0
Dureza	Shore A	DIN 53505	45±3
Alongamento à rutura	%	DIN 53504	250
Resistência à tração	N/mm²	DIN 53504	1,5
Resistência ao rasgão	N/mm	DIN 5315	Não determinado
Capacidade de recuperação elástica	%	–	> 70
Módulo de elasticidade a 100% alongamento	N/mm²	–	0,9
Resistência à temperatura	°C	–	-40°C a +80°C
COV	Não determinado		

A.5 PMMA specs

TECHNICAL SHEET Setacryl® and Polarlite®

Physical-chemical properties.

The following table reports the characteristic properties of standard Setacryl® and Polarlite® sheets; coloured opaline sheets have different physical-chemical properties (in addition to optic ones, obviously) depending on the type.

	Method	Unit Of measurement	Values
Physical Properties			
Density	ISO 1183	g/cm3	1.19
Water absorption after 24 h	ISO R 62/DIN53495	%	0.3
Optic Properties			
Transmittance (on colourless material)	ISO 4892-1 DIN 5036	%	92
Haze (on colourless material)	ASTM D 1003	%	< 0.5
Refraction index (on colourless material)	ISO 4892/DIN 53491	°C	1.49
Mechanical Properties			
Coefficient of elasticity due to pulling stress 23°C	ISO 527-2/1 B/1	MPa	3300
Ultimate elongation 23°C	ISO 527-2/1 B/5	%	5
Tensile strength 23°C	ISO 527-2/1 B/5	MPa	76
Flexing resistance	ISO 178	MPa	110
Compression resistance	ISO 604	MPa	110
IZOD impact resistance with notch	ISO 180/ 1 A	kJ/m2	1.4
Charpy impact resistance without notch	ISO 179/ 1	kJ/m2	13
Abrasion resistance	ISO 14782	%	0.5 to 1
Maximum allowed tension		MPa	5-7
Minimum cold curvature radius		mm	330 x thickness.
Thermal Properties			
Softening time (Vicat)	ISO R 306 Method A 50	°C	>108
Deflection time (HDT)	ISO 75/A	°C	>102
Maximum running time		°C	80
Linear Expansion Coefficient	VDE 0304/1		7
Thermal conductivity	DIN 52612	W/m/°C	0.17
Fire behaviour			
Self-ignition temperature	DIN 51794	°C	430 c.a.
Fire behaviour	NF P 9250		M4
Other Properties			
Poisson coefficient	ISO 527 -1		0.39
Thermoforming Parameters			
Thermoforming interval		°C	140-190
Heating furnace temperature		°C	130-180
Maximum heating temperature		°C	200
Shrinkage after heating		%	2.5 max

This information is given as a guide and does not represent the technical specifications of the materials and therefore does not imply any responsibility on the part of MADREPERLA SpA

A.6 Experimental Results of Configuration A/Pecol adhesive

Displacement [mm]	Force with Pecol [N]			Average	SD
	Sample 1	Sample 2	Sample 3		
0	0	0	0	0	0
0,082	13,75	22,813	29,38	21,98	6,41
0,166	42,81	48,44	57,5	49,58	6,05
0,249	71,25	76,88	86,88	78,34	6,46
0,332	98,75	104,38	114,38	105,84	6,46
0,416	127,81	130,31	144,69	134,27	7,44
0,499	155	155,63	172,81	161,15	8,25
0,582	182,19	185,63	200,31	189,38	7,86
0,666	211,25	212,81	230,63	218,23	8,79
0,749	239,38	240,94	258,13	246,15	8,50
0,832	269,69	267,19	288,13	275,00	9,34
0,916	295,94	295,66	316,25	302,62	9,64
0,999	324,69	324,38	346,25	331,77	10,24
1,082	353,75	351,25	375	360,00	10,66
1,166	381,88	378,44	403,75	388,02	11,21
1,249	410,31	408,75	433,44	417,50	11,29
1,332	437,81	435,94	463,44	445,73	12,55
1,416	465,94	464,38	493,44	474,59	13,35
1,499	492,81	492,19	522,5	502,50	14,14
1,582	519,38	519,06	552,5	530,31	15,69
1,666	546,88	547,81	581,56	558,75	16,13

	F=300N			Average	SD
Displacement	0,928	0,928	0,867	0,908	0,035
Rotation	1,266	1,273	1,283	1,274	0,009

A.7 Experimental Results of Configuration A/Epoxy adhesive

Displacement [mm]	Force with Epoxy [N]			Average	SD
	Sample 1	Sample 2	Sample 3		
0	0	0	0	0	0
0,082	91,25	90,31	88,12	89,89	1,606
0,166	181,56	188,44	178,75	182,92	4,985
0,249	246,88	286,25	274,69	269,27	20,236
0,332	344,69	385,31	369,38	366,46	20,467
0,416	443,13	483,13	464,06	463,44	20,007
0,499	541,88	583,13	558,13	561,05	20,779
0,582	641,88	683,75	654,38	660,00	21,494
0,666	742,81	785	751,88	759,90	22,208
	F=300N			Average	DP
Displacement	0,294	0,261	0,271	0,275	0,017
Rotation	0,364	0,765	0,571	0,567	0,201

A.8 Experimental Results of Configuration B/Pecol adhesive

Displacement [mm]	Force with Pecol [N]			Average	SD
	Sample 1	Sample 2	Sample 3		
0	0	0	0	0	0
0,082	8,13	8,75	10	8,96	0,95
0,166	21,56	16,88	17,81	18,75	2,48
0,249	33,13	29,06	33,44	31,88	2,44
0,332	46,56	42,5	41,88	43,65	2,54
0,416	59,38	56,56	54,69	56,88	2,36
0,499	73,44	69,38	66,25	69,69	3,61
0,582	86,88	82,81	81,56	83,75	2,78
0,666	99,69	95,625	89,38	94,90	5,19
0,749	114,06	107,81	102,81	108,23	5,64
0,832	126,88	121,88	116,25	121,67	5,32
0,916	140,63	132,81	128,44	133,96	6,18
0,999	155	146,25	141,25	147,50	6,96
1,082	167,81	159,69	153,44	160,31	7,21
1,166	180,56	171,88	165,94	172,79	7,35
1,249	193,75	185	179,38	186,04	7,24
1,332	208,125	197,5	192,19	199,27	8,11
1,416	222,19	209,06	205	212,08	8,98
1,499	235,63	223,13	218,13	225,63	9,01
1,582	248,13	236,25	230,94	238,44	8,80
1,666	262,5	249,69	244,06	252,08	9,45
1,749	275,31	262,19	256,88	264,79	9,49
1,832	288,75	274,69	269,06	277,50	10,14
1,916	303,44	288,75	281,88	291,36	11,01
1,999	315	299,69	294,38	303,02	10,71
2,082	327,81	313,13	305,63	315,52	11,28
2,166	341,25	325,63	318,75	328,54	11,53
2,249	353,13	339,06	330,94	341,04	11,23
2,332	365,63	351,25	341,88	352,92	11,96
2,416	378,13	364,38	353,44	365,32	12,37
2,499	390	375,94	365,63	377,19	12,23
2,582	402,19	390	375,94	389,38	13,14
2,666	414,69	403,13	387,5	401,77	13,65
	F=300N			Average	SD
Displacement	1,896	2	2,04	1,979	0,074
Rotation	2,225	1,955	1,991	2,057	0,147

A.9 Experimental Results of Configuration B/Epoxy adhesive

Displacement [mm]	Force with Epoxy [N]			Average	SD
	Sample 1	Sample 2	Sample 3		
0	0	0	0	0	0
0,082	10,94	8,13	9,38	9,48	1,41
0,166	25,31	20,94	24,38	23,54	2,30
0,249	42,19	36,88	40,31	39,79	2,69
0,332	56,88	51,88	56,25	55,00	2,72
0,416	71,56	65,31	71,25	69,37	3,52
0,499	87,19	82,19	86,88	85,42	2,80
0,582	102,5	96,56	103,44	100,83	3,73
0,666	119,06	112,5	118,75	116,77	3,70
0,749	135	128,13	134,69	132,61	3,88
0,832	150,63	144,38	150,94	148,65	3,70
0,916	166,25	159,69	166,88	164,27	3,98
0,999	182,5	175,64	182,81	180,32	4,05
1,082	198,44	190,63	198,44	195,84	4,51
1,166	214,38	205,94	214,38	211,57	4,87
1,249	231,89	222,19	230	228,03	5,14
1,332	245,63	237,5	245,56	242,90	4,67
1,416	263,44	252,81	262,5	259,58	5,88
1,499	278,75	269,06	278,13	275,31	5,42
1,582	294,38	284,69	294,69	291,25	5,69
1,666	310	300,63	311,56	307,40	5,91
1,749	325,63	316,88	325,63	322,71	5,05
1,832	340	332,5	343,13	338,54	5,46
1,916	354,69	347,5	359,69	353,96	6,13
1,999	368,44	362,5	374,38	368,44	5,94
2,082	384,38	379,69	390,94	385,00	5,65
2,166	399,38	396,25	406,56	400,73	5,29
2,249	412,5	411,25	421,88	415,21	5,81
2,332	426,25	426,88	438,13	430,42	6,68
2,416	440,31	442,81	451,88	445,00	6,09
2,499	452,81	457,81	469,69	460,10	8,67
2,582	466,25	474,96	486,25	475,82	10,03
2,666	480	489,06	500,94	490,00	10,50
	F=300N			Average	SD
Displacement	1,612	1,663	1,608	1,628	0,031
Rotation	1,915	1,517	1,643	1,692	0,203

A.10 Experimental Results of Configuration C/Pecol adhesive

Displacement [mm]	Force with Pecol [N]			Average	SD
	Sample 1	Sample 2	Sample 3		
0	0	0	0	0	0
0,082	10,94	12,5	15,63	13,02	2,39
0,166	27,81	26,88	29,69	28,13	1,43
0,249	48,13	44,69	38,75	43,86	4,75
0,332	68,13	64,69	50,31	61,04	9,45
0,416	86,88	84,06	60,63	77,19	14,41
0,499	108,75	102,19	72,19	94,38	19,49
0,582	129,31	121,25	88,75	113,10	21,47
0,666	150,31	141,88	106,13	132,77	23,46
0,749	170,63	161,25	126,56	152,81	23,21
0,832	191,88	180,63	144,06	172,19	25,00
0,916	213,44	200,94	162,5	192,29	21,68
0,999	234,69	220,94	185	213,54	25,66
1,082	253,75	238,44	203,75	231,98	25,62
1,166	274,06	259,06	224,38	252,50	25,48
1,249	294,06	279,06	244,38	272,50	25,48
1,332	314,06	297,81	265,63	292,50	24,65
1,416	335,94	318,13	285,31	313,13	25,68
1,499	356,25	338,75	305	333,33	26,05
1,582	376,56	357,19	325,31	353,02	25,88
1,666	396,56	380,31	345,31	374,06	26,19
1,749	416,56	398,13	365	393,23	26,13
1,832	436,56	417,81	383,44	412,60	26,94
1,916	455	437,5	403,13	431,88	26,39
1,999	472,81	456,88	420,94	450,21	26,57
	F=300N			Average	SD
Displacement	1,274	1,341	1,478	1,364	0,104
Rotation	1,403	1,61	1,361	1,46	0,133

A.11 Experimental Results of Configuration C/Epoxy adhesive

Displacement [mm]	Force with Epoxy [N]			Average	SD
	Sample 1	Sample 2	Sample 3		
0	0	0	0	0	0
0,082	14,38	6,875	15,63	12,30	4,74
0,166	26,44	25,94	29,69	27,36	2,04
0,249	35,38	52,19	38,75	42,11	8,89
0,332	49,75	76,25	50,31	58,77	15,14
0,416	63,75	102,81	60,63	75,73	23,50
0,499	79,68	128,13	72,19	93,33	30,37
0,582	99,06	154,69	88,75	114,17	35,47
0,666	116,88	179,68	108,13	134,90	39,03
0,749	136,25	205,31	126,56	156,04	42,94
0,832	156,88	231,56	144,06	177,50	47,25
0,916	175,94	258,44	162,5	198,96	51,95
0,999	194,69	283,13	185	220,94	54,08
1,082	215,94	309,38	203,75	243,02	57,79
1,166	238,13	335,63	224,34	266,03	60,67
1,249	260	360	244,38	288,13	62,73
1,332	285,31	385,94	265,62	312,29	64,54
1,416	305	410	285,31	333,44	67,03
1,499	325,31	434,06	305	354,79	69,40
1,582	345,31	458,44	325,31	376,35	71,79
1,666	365	482,19	345,31	397,50	74,00
1,749	383,44	504,38	365	417,61	75,71
1,832	403,13	525,94	383,44	437,50	77,22
1,916	420,94	546,56	403,13	456,88	78,18
1,999	436,88	566,88	420,94	474,90	80,05
	F=300N			Average	SD
Displacement	1,395	1,052	1,478	1,308	0,226
Rotation	0,92	1,514	1,483	1,306	0,334